

Correct and Certify: A New Approach to Self-Supervised 3D-Object Perception

Rajat Talak, Lisa Peng, and Luca Carlone

Abstract—We consider an object pose estimation and model fitting problem, where —given a partial point cloud of an object—the goal is to estimate the object pose by fitting a CAD model to the sensor data. We solve this problem by combining (i) a semantic keypoint-based pose estimation model, (ii) a novel self-supervised training approach, and (iii) a certification procedure, that not only verifies whether the output produced by the model is correct or not, but also flags uniqueness of the produced solution. The semantic keypoint detector model is initially trained in simulation and does not perform well on real-data due to the domain gap. Our self-supervised training procedure uses a *corrector* and a *certification* module to improve the detector. The corrector module corrects the detected keypoints to compensate for the domain gap, and is implemented as a declarative layer, for which we develop a simple differentiation rule. The certification module declares whether the corrected output produced by the model is certifiable (*i.e.*, correct) or not. At each iteration, the approach optimizes over the loss induced only by the certifiable input-output pairs. As training progresses, we see that the fraction of outputs that are certifiable increases, eventually reaching near 100% in many cases. We conduct extensive experiments to evaluate the performance of the corrector, the certification, and the proposed self-supervised training using the ShapeNet and YCB datasets, and show the proposed approach achieves performance comparable to fully supervised baselines while not requiring pose or keypoint supervision on real data.

I. INTRODUCTION

Object pose estimation from 3D point clouds is an important problem in robot perception, with applications including industrial robotics [3]–[6], self-driving cars [7]–[13], and domestic robotics [1], [2], [14]–[17]. Availability of pose-annotated datasets has fueled recent progress towards solving this problem [1]–[3], [7]–[9]. Many approaches have been proposed that regress the pose from the inputs and train well under full supervision [10]–[13], [18]–[25]. Yet, several challenges such as scalability to unseen objects and robustness to occlusions remain open even under such supervised settings [26]–[28].

For robotic applications, however, annotated training data is not only costly to obtain, but also robot-dependent, since a change in placement of the sensor/camera (e.g. from the top of a self-driving car to the head of a quadruped robot) will distort the predictions produced by the trained model. Though realistic simulators provide a partial answer to this problem [4], [29]–[31], a sim2real gap remains that needs to be tackled. Very few works have been proposed to solve the pose estimation and model fitting problem in a self-supervised manner [32]–[35].

The authors are with the Laboratory of Information and Decision Systems (LIDS), Massachusetts Institute of Technology, Cambridge, MA 02139, USA. Corresponding author: Rajat Talak (email: talak@mit.edu)

This work was partially funded by ARL DCIST CRA W911NF-17-2-0181, ONR RAIDER N00014-18-1-2828, and NSF CAREER award “Certifiable Perception for Autonomous Cyber-Physical Systems”.

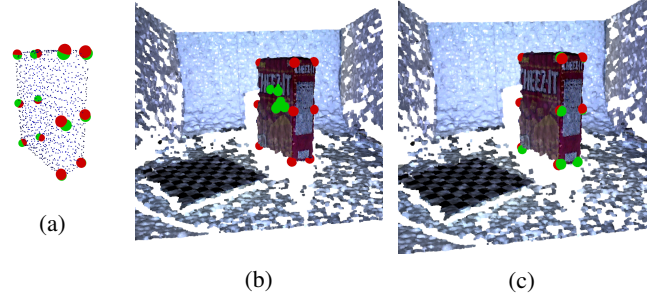


Fig. 1: Illustration of the result of our self-supervised “corrector + certification” training. Semantic keypoints (green) predicted by a simulation-trained keypoint detector (a) work well on a simulated object point cloud, but (b) deviate from the ground truth keypoints (red) on real-world RGB-D point clouds due to the sim-to-real gap. (c) Our keypoints (green) predicted by the keypoint detector, plus corrector, match the ground truth on the real-world RGB-D point cloud, after self-supervised training with certification. Data from the YCB dataset [1], [2].

Another major challenge is the trust and certifiability of neural network based approaches. Robot perception requires models that can be relied upon for the robot to act safely. Perception failures can lead to catastrophic consequences including loss of life [36]–[39]. It is also important in many cases to guarantee that the output produced by the model is not only correct, but is also the unique solution to the problem being solved (e.g., there may be more than one way to fit an object CAD model to a visible point cloud of an object, if it is sufficiently occluded). No notion of certifiability, to the best of our knowledge, has been proposed to meet this requirement.

Self-supervised training and self-certification are two pivotal hurdles in scaling current computer vision models to safety-critical robotics applications. *We, therefore, need a way to take a model trained in simulation, where full supervision is available, and generalize it to another dataset, that is unlabeled, possibly with further training that is self-supervised. We simultaneously need to provide certification guarantees on the correctness – and possibly uniqueness – of the outputs produced.*

We propose a way to do this for a semantic keypoint-based pose estimation and model fitting problem [21], [40]–[43]. In it, we are given a keypoint detector that detects semantic keypoints from a point cloud picturing an object; the detected keypoints are used to register the object model, thereby estimating the object pose. We assume that the semantic keypoint detector can be trained in simulation, with full supervision of keypoints and ground truth poses. However, the gap between the simulated data and the real-world data is such that the detector fails to

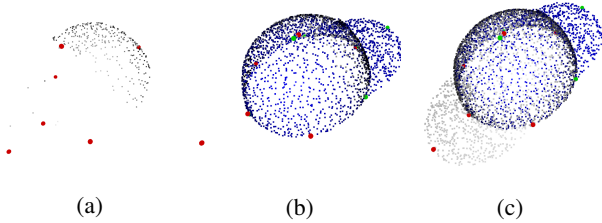


Fig. 2: Example of degeneracy when fitting a point cloud of a ‘cap’ (object in ShapeNet [46]) with its CAD model, represented as a full point cloud. (a) input depth point cloud of the object (gray), (b) predicted object model (blue), and (c) predicted object model (blue) and the ground truth object (gray). Also shown are the ground truth keypoints (red) and detected keypoints (green).

estimate the semantic keypoints with good accuracy—and hence is unable to provide good pose estimates—on real data.

We propose a self-supervised training method, that uses a *corrector module*, to correct the detected keypoints to compensate for the domain gap, and a *certification module*, that certifies if the obtained pose and predicted object model is correct or not, for the given the input. The self-supervised training proceeds by training only on the certifiable input-output pairs. As training progresses, the certified pairs produced by the model increase, eventually resulting in fully trained model that can detect keypoints and estimate poses on the real-world dataset to a good accuracy; see Fig. 1 for an illustration.

The corrector module is implemented as a declarative layer [44], [45]. It takes in the detected keypoints and produces a correction, by solving a non-linear, non-convex optimization problem. Although the corrector optimization problem is hard to analyze, we show that it can be differentiated through very easily. We provide an exact analytical expression of the gradient of the output (the correction), given the input (detected keypoints) to the corrector, which we use to implement back-propagation. We also implement a *batch gradient descent* that solves a batch of corrector optimization problems in parallel on GPU, thereby speeding up the forward pass.

We develop a notion of *certifiability* that asserts whether the output of the model matches the input data. Then we also propose a new notion of *strong certifiability* wherein the model can check if there are multiple ways to fit the object CAD model to the input (what we call a *degenerate* instance), in the forward pass. This is useful to assert whether the model predicted pose and CAD model fit is unique or not, for the given input. Fig. 2 shows an example of degeneracy.

We conduct extensive experiments to evaluate the performance of the corrector, certification, and the proposed self-supervised training. Experimental analysis shows that the corrector is able to correct high-variance, added perturbations to the semantic keypoints. Then, we test the self-supervised training on (i) a generated dataset using ShapeNet objects [46] and (ii) the YCB dataset consisting of RGB-D images [1], [2]. In both cases, we observe that while the simulation-trained models perform poorly, our self-supervised training

is able to successfully train it further and achieves comparable performance to a fully supervised baseline, despite not relying on real-world labels. We also see that our implementation of strong certifiability enables the trained model to ascertain both the correctness and uniqueness of the model output.

II. RELATED WORK

Self-Supervised Pose Estimation. Very few works have tackled the problem of self-supervised pose estimation and model fitting. In [32], [33], a pose estimation model is first trained on synthetic RGB-D data, and then refined further with self-supervised training on real, unannotated data. Differentiable rendering provides for the required supervision signal. Student-teacher iterative schemes are proposed in [47] and [48] to bridge the domain gap in pose estimation. Another approach is to extract a pose-invariant feature, thereby canonizing only its shape [49], and using it for supervision. Zakharov *et al.* [34] utilize differentiable rendering of signed distance fields of objects, along with normalized object coordinate spaces [49], to learn 9D cuboids in a self-supervised manner. Li *et al.* [50] extract an SE(3)-invariant feature, which works as a canonical object, and uses it to supervise training with a Chamfer loss. He *et al.* [51] extract a pose and scale invariant feature, and uses it for deforming a template mesh of an object. Doing this, it is able to propose a category-level object pose and size estimation architecture. The training, however, uses ground-truth registered coarse object point cloud for supervision. Deng *et al.* [35] proposes a way to self-supervise pose estimation by interacting with the objects in the environment. The pose estimator gets trained on the data collected autonomously by a manipulator. These approaches use pose-invariant features, differentiable rendering, or robot action to provide the supervision signal. In contrast, we show that, using a fixed set of semantic keypoints, a simple corrector module, in conjunction with a certifier, can provide the necessary supervision.

Registration and Feature-based Methods. Classical methods for registration [52]–[58] can also be used for pose estimation and model fitting with point clouds. In this case, robustness and outlier rejection are of concern. Robust and certifiable approaches have recently been proposed [59]–[64], but they still assume the availability of a suitable feature detection front-end. Learning-based registration approaches that jointly extract features and estimate poses have been proposed [48], [65]–[80], and yet only a few can be trained in a self-supervised manner. A semi-supervised approach that uses ground-truth poses for feature learning is proposed in [73]. A weakly-supervised approach, using a triplet loss, is developed in [78]. Self-supervised partial-to-partial scene registration is considered in [79], [80]. In particular, Banani *et al.* [80] use the fact that two successive frames inherit some geometric and photometric consistency, and leverage differentiable rendering to implement the training loss. A teacher-student-verifier framework for joint feature learning and registration is considered in [48]. The performance guarantees provided by feature-based methods mostly focus on the optimality of the registration [81].

Certification. Certifying correctness of the model output is crucial for safety-critical and high-integrity applications. A

certifiable algorithm returns a solution and also provides a certificate of its optimality and possibly correctness [81]–[83]. Certifiable algorithms have been devised for several geometric perception problems [59], [62], [84], [85], where the duality gap serves as the certificate. We extend this definition to learning models, which can deviate from the intended behavior in practice. We also define the notion of strong certifiability, where in we require the model to output another flag, if it thinks the problem has multiple solutions. In this work, we also use the notion of certification for self-supervised training.

III. PROBLEM STATEMENT AND CERTIFICATION

A. Problem Statement

Certifiable Pose Estimation and Model Fitting. We are given a partial point cloud \mathbf{X} of an object, which we assume has been segmented from the background. We are also given a CAD model of the object we want to detect, with marked semantic keypoints; we use \mathbf{B} and \mathbf{b} to denote the CAD model and its annotated semantic keypoints. Certifiable pose estimation and model fitting then aims at computing the object pose $(\hat{\mathbf{R}}, \hat{\mathbf{t}})$ and a (registered) CAD model $\hat{\mathbf{X}}$ that fits \mathbf{X} , together with a *certificate of correctness* for the solution.

We consider a semantic keypoint-based pose estimation and model fitting architecture (see Fig. 3). In it, semantic keypoints are first detected from the input point cloud \mathbf{X} , and are then used to register the object CAD model \mathbf{B} to the input. The registration block estimates the object pose by solving

$$\hat{\mathbf{R}}, \hat{\mathbf{t}} = \arg \min_{\mathbf{R} \in \text{SO}(3), \mathbf{t} \in \mathbb{R}^3} \sum_{i=1}^N \|\hat{\mathbf{y}}[i] - \mathbf{R}\mathbf{b}[i] - \mathbf{t}\|_2^2, \quad (1)$$

where $\hat{\mathbf{y}}[i]$ and $\mathbf{b}[i]$ denote the i -th detected and model keypoints, respectively. We use a semantic keypoint-based model because the semantic keypoints represent various semantic regions of the object, and as we shall see, they can help in certifying the correctness of the object pose and the model fit.

Unannotated Data and Self-supervision. For training, we are given a real-world dataset of partial point clouds of objects, segmented from a scene. No pose or keypoint annotation is available on the real-world dataset. Annotated simulation data, however, is available and can be used to initialize weights of the keypoint detector. Therefore, we assume that we are given a semantic keypoint detector that is trained in simulation. This detector, however, does not perform well on the real-world dataset of segmented, object point clouds. The goal is to modify, correct, and/or further train the semantic keypoint detector, and the baseline architecture in Fig. 3, to enable it to predict the correct keypoints on the real-world data, thereby enabling successful pose estimation and model fitting.

Problem 1 (Self-supervised, Certifiable Pose Estimation and Model Fitting Problem). *Propose a method to train the semantic-keypoint-based pose estimation and model fitting architecture (see Fig. 3), when the training data consists of partial point clouds of an object, segmented from a scene, with no pose or semantic keypoint annotations. The model has to provide a certificate of correctness for the resulting outputs.*

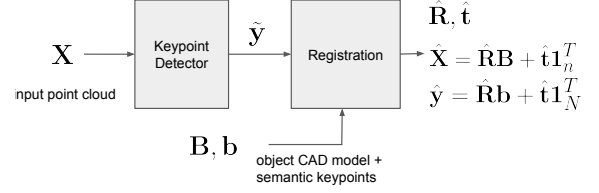


Fig. 3: Standard architecture for semantic-keypoint-based pose estimation and model fitting.

B. Certifiability

This section clarifies the nature of the “certificate of correctness” required by Problem 1. Here we introduce the notion of certifiability in full generality, while we tailor it to the pose estimation and model fitting in Section IV.

Certifiability and Strong Certifiability. Let $\mathcal{P}(\mathbf{X})$ be a problem that is parameterized by input \mathbf{X} , and let $\mathcal{S}(\mathbf{X}) \subset \mathcal{Z}$ denote the set of all solutions to $\mathcal{P}(\mathbf{X})$, within the output space \mathcal{Z} (i.e., \mathcal{Z} is the set of possible answers an algorithm solving \mathcal{P} can provide, while $\mathcal{S}(\mathbf{X})$ are the correct answers). We consider \mathcal{Z} to be a metric space with metric d , i.e., for two outputs $z, z' \in \mathcal{Z}$, the metric $d(z, z')$ quantifies the distance between z and z' . We define the following certificates.

Definition 1 (Correctness and Non-Degeneracy Certificates). *For a problem \mathcal{P} , instantiated with input \mathbf{X} , the certificate of correctness is a boolean condition defined as*

$$\text{Correctness}[\mathcal{P}, \mathbf{X}](z) = \mathbb{I}\{z \in \mathcal{S}(\mathbf{X})\}, \quad (2)$$

for all outputs $z \in \mathcal{Z}$ produced by a model to solve \mathcal{P} . A certificate of non-degeneracy, on the other hand, is defined as

$$\text{NonDegeneracy}[\mathcal{P}, \mathbf{X}] = \mathbb{I}\{\text{Diam}[\mathcal{S}(\mathbf{X})] < \delta\}, \quad (3)$$

where $\text{Diam}[\mathcal{S}(\mathbf{X})] = \max_{z, z' \in \mathcal{S}(\mathbf{X})} d(z, z')$ denotes the diameter of the solution space $\mathcal{S}(\mathbf{X})$, and δ is a small constant.

Example. In pose estimation and model fitting, the input is the given point cloud \mathbf{X} , while the output space \mathcal{Z} is the space of all tuples $(\hat{\mathbf{y}}, \hat{\mathbf{X}})$ of the predicted model keypoints $\hat{\mathbf{y}}$ and the predicted model fit $\hat{\mathbf{X}}$ (see Fig. 3) an algorithm can return. The metric d is the Chamfer loss. The solution space $\mathcal{S}(\mathbf{X})$ is the set of outputs $(\hat{\mathbf{y}}, \hat{\mathbf{X}})$ such that $\hat{\mathbf{X}}$ correctly aligns with the input \mathbf{X} . An output that correctly aligns the CAD model to the input cloud is certifiably correct as per eq. (2).

The notion of non-degeneracy, instead, is related to the correct alignment being unique. In order to understand eq. (3), consider the following example. We are given a point cloud of a mug that is otherwise symmetric, except for the handle. If the input point cloud \mathbf{X} of the mug is missing the handle because of the camera viewing angle, there can be more than one correct pose $(\hat{\mathbf{R}}, \hat{\mathbf{t}})$ and model fit $\hat{\mathbf{X}}$. In other words, there is more than one solution to the problem, for the given input, and $\text{Diam}[\mathcal{S}(\mathbf{X})]$ is large. In case the handle is visible, instead, the problem becomes non-degenerate, meaning that it is possible to compute a unique solution (up to noise); see Fig. 2.

We use the correctness and non-degeneracy certificates to define certifiability and strong certifiability for a model.

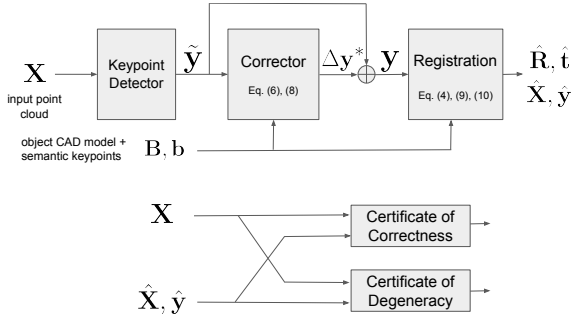


Fig. 4: Proposed semantic-keypoint-based pose estimation and model fitting architecture with *corrector* and *certification*.

Definition 2 (Certifiability and Strong Certifiability). *Let \mathcal{M} be a model that is trained to solve \mathcal{P} for an input \mathbf{X} , i.e., \mathcal{M} produces a solution $z = \mathcal{M}(\mathbf{X})$ to problem $\mathcal{P}(\mathbf{X})$, given input \mathbf{X} . We say that \mathcal{M} is certifiable if it can also produce a certificate of correctness for all inputs \mathbf{X} . We say that a model \mathcal{M} is strongly certifiable, if it can produce both a certificate of correctness and a certificate of non-degeneracy, for all \mathbf{X} .*

IV. ARCHITECTURE

This section describes the proposed architecture which is also illustrated in Fig. 4. We add two modules to the standard semantic-keypoint-based architecture in Fig. 3: a corrector and a certifier. The corrector module corrects perturbations in the detected semantic keypoints (e.g., due to the sim-to-real gap) and is implemented as a declarative layer. The certifier contains implementations of eqs. (2)-(3) and is used to selected correct registration results that can be then used for self-training.

A. Keypoint Detector

We implement the keypoint detector as a trainable regression model, that uses a neural architecture for point cloud data; in our experiments, we use PointNet++ [86], [87] and point transformer [88]. The architecture takes a point cloud $\mathbf{X} \in \mathbb{R}^{3 \times n}$ as input, and estimates semantic keypoints $\tilde{\mathbf{y}} \in \mathbb{R}^{3 \times N}$, where n is the number of points in the point cloud and N is the number of keypoints. The keypoint detector is initially trained in simulation, on a set of artificially generated point clouds of the object and the corresponding semantic keypoints.

B. Keypoint Corrector

The keypoint corrector takes the estimated semantic keypoints $\tilde{\mathbf{y}} \in \mathbb{R}^{3 \times N}$ —produced by the keypoint detector—as input, and outputs a correction term $\Delta \mathbf{y} \in \mathbb{R}^{3 \times n}$ to the keypoints. The corrected keypoints are then given by

$$\mathbf{y} = \tilde{\mathbf{y}} + \Delta \mathbf{y}. \quad (4)$$

The correction term $\Delta \mathbf{y}^*$ is obtained as a solution to the *corrector optimization problem*. First, we introduce some notation. Let $\mathbf{R}(\Delta \mathbf{y})$ and $\mathbf{t}(\Delta \mathbf{y})$ denote the optimal solution to the keypoint-based pose estimation problem (1), but with the keypoints $\mathbf{y} = \tilde{\mathbf{y}} + \Delta \mathbf{y}$, instead of $\tilde{\mathbf{y}}$ in (1). Further, let

the predicted object model $\hat{\mathbf{X}}$ and predicted model keypoints $\hat{\mathbf{y}}$, for a given correction term $\Delta \mathbf{y}$, be:

$$\hat{\mathbf{X}} = \mathbf{R}(\Delta \mathbf{y})\mathbf{B} + \mathbf{t}(\Delta \mathbf{y})\mathbf{1}_n^\top \quad \text{and} \quad \hat{\mathbf{y}} = \mathbf{R}(\Delta \mathbf{y})\mathbf{b} + \mathbf{t}(\Delta \mathbf{y})\mathbf{1}_N^\top, \quad (5)$$

where \mathbf{B} denotes the object model, \mathbf{b} the model keypoints, and $\mathbf{1}_N$ denotes the N -vector with all entries equal to 1.

Corrector Optimization Problem. The correction $\Delta \mathbf{y}$ is optimized so that the predicted object model $\hat{\mathbf{X}}$ and the model keypoints $\hat{\mathbf{y}}$ are aligned to the input point cloud \mathbf{X} and the corrected keypoints \mathbf{y} :

$$\begin{aligned} \underset{\Delta \mathbf{y}}{\text{minimize}} \quad & \text{ch}_{1/2}(\mathbf{X}, \hat{\mathbf{X}}) + \gamma \|\mathbf{y} - \hat{\mathbf{y}}\|_2^2, \\ \text{subject to} \quad & \hat{\mathbf{X}} = \mathbf{R}(\Delta \mathbf{y})\mathbf{B} + \mathbf{t}(\Delta \mathbf{y})\mathbf{1}_n^\top, \\ & \hat{\mathbf{y}} = \mathbf{R}(\Delta \mathbf{y})\mathbf{b} + \mathbf{t}(\Delta \mathbf{y})\mathbf{1}_N^\top. \end{aligned} \quad (6)$$

where γ is a positive constant and $\text{ch}_{1/2}(\mathbf{X}, \hat{\mathbf{X}})$ is the half-Chamfer loss given by

$$\text{ch}_{1/2}(\mathbf{X}, \hat{\mathbf{X}}) = \frac{1}{|\mathbf{X}|} \sum_{\mathbf{x} \in \mathbf{X}} \min_{\hat{\mathbf{x}} \in \hat{\mathbf{X}}} \|\mathbf{x} - \hat{\mathbf{x}}\|_2^2, \quad (7)$$

which sums over only the distances between a point \mathbf{x} in the input point cloud \mathbf{X} with a nearest point $\hat{\mathbf{x}}$ in the predicted object model $\hat{\mathbf{X}}$. Here, $|\mathbf{X}|$ denotes the number of points in \mathbf{X} . The use of the half-Chamfer loss is motivated by the fact that the input point cloud \mathbf{X} is typically only partially visible, due the camera viewpoint and potential occlusions.

Gradient Computation. The proposed model contains a neural architecture (keypoint detector) and two declarative layers (keypoint corrector and keypoint-based registration). In order to train using back-propagation, we need to compute the gradient of the output viz-a-viz the input for each of the layers in our architecture. The registration block solves (1). Computation of this solution involves linear operations and SVD computation [89]–[91]. This is easily implemented as a differentiable layer in PyTorch [92].

We now show that the corrector optimization problem (6), although being non-linear and non-convex, heeds to a very simple differentiation (proof in Appendix A).

Theorem 3. *The gradient of the correction $\Delta \mathbf{y}^*$ with respect to the estimated keypoints $\tilde{\mathbf{y}}$ is the negative identity, i.e.,*

$$\partial \Delta \mathbf{y}^* / \partial \tilde{\mathbf{y}} = -\mathbf{I}. \quad (8)$$

Intuitively, the result is easy to see. In (6), the correction term $\Delta \mathbf{y}$ always appears in conjunction with $\tilde{\mathbf{y}}$, and that too, in the form $\tilde{\mathbf{y}} + \Delta \mathbf{y}$. Therefore, a small change of $d\tilde{\mathbf{y}}$ in $\tilde{\mathbf{y}}$, namely $\tilde{\mathbf{y}} \rightarrow \tilde{\mathbf{y}} + d\tilde{\mathbf{y}}$ in (6), which may cause $\Delta \mathbf{y}^*$ to stray away from the optima, will certainly be compensated by a change in $\Delta \mathbf{y}$ by the exact opposite amount, namely, $d\Delta \mathbf{y} = -d\tilde{\mathbf{y}}$. If nothing else, this new correction, namely $\Delta \mathbf{y}^* - d\tilde{\mathbf{y}}$, is sure to retain the optimality in (6), for the new detected keypoints $\tilde{\mathbf{y}} + d\tilde{\mathbf{y}}$. This, intuitively implies the result $\partial \Delta \mathbf{y}^* / \partial \tilde{\mathbf{y}} = -\mathbf{I}$.

Theorem 3 makes the implementation of back-propagation for the corrector layer very simple. This also frees us to chose any optimization algorithm to solve the problem in (6), in the forward pass. We implement *batch gradient descent*, that solves a batch of corrector optimization problems in parallel on GPU, thereby speeding up forward pass; see details in Appendix B.

C. Registration

Given $\Delta \mathbf{y}^*$ to be the optimal or approximate solution to (6), the pipeline predicts the pose, the object model fit, and the model keypoints to be:

$$\hat{\mathbf{R}} = \mathbf{R}(\Delta \mathbf{y}^*), \quad \hat{\mathbf{t}} = \mathbf{t}(\Delta \mathbf{y}^*), \quad (9)$$

$$\hat{\mathbf{X}} = \hat{\mathbf{R}}\mathbf{B} + \hat{\mathbf{t}}\mathbf{1}_n, \quad \hat{\mathbf{y}} = \hat{\mathbf{R}}\mathbf{b} + \hat{\mathbf{t}}\mathbf{1}_N. \quad (10)$$

This is implemented using a differentiable layer (1) that obtains $\mathbf{R}(\Delta \mathbf{y}^*)$ and $\mathbf{t}(\Delta \mathbf{y}^*)$, given the outputs $(\Delta \mathbf{y}^*, \tilde{\mathbf{y}})$ produced by the corrector and the detector. The reason for re-computing the rotation and translation estimates is that it results in a clean implementation of the back-propagation, for a marginal forward computation overhead.

D. Certification

To enable certification and strong certification (Definition 2), we need to provide certificates of correctness and degeneracy. The computation of these certificates must only involve the inputs (*e.g.*, \mathbf{X}) and the model predictions (*e.g.*, $\hat{\mathbf{R}}, \hat{\mathbf{t}}, \hat{\mathbf{X}}, \hat{\mathbf{y}}$).

Certificate of Correctness. Our model predicts object model $\hat{\mathbf{X}}$, which is represented as a dense point cloud. We can determine the correctness of the prediction by comparing $\hat{\mathbf{X}}$ with the input point cloud \mathbf{X} , which is a segmented, partial point cloud of the object. We implement the certificate of correctness using the max-Chamfer loss:

$$c(\mathbf{X}, \hat{\mathbf{X}}) = \mathbb{I} \left\{ \max_{\mathbf{x} \in \mathbf{X}} \max_{\hat{\mathbf{x}} \in \hat{\mathbf{X}}} \|\mathbf{x} - \hat{\mathbf{x}}\|_2 < \epsilon \right\}, \quad (11)$$

where $\epsilon > 0$ is a given hyper-parameter. We declare input-output pair to be certifiable (*i.e.*, correct) if $c(\mathbf{X}, \hat{\mathbf{X}}) = 1$, and not certifiable otherwise. In words, condition (11) evaluates the quality of fit by checking that all points in the input \mathbf{X} are within a distance ϵ from points in the predicted model $\hat{\mathbf{X}}$.

Certificate of Non-Degeneracy. For an input point cloud \mathbf{X} , of an object, to be considered non-degenerate we require that key semantic features (or, more precisely, keypoints) of the object must be visible in \mathbf{X} . For example, a partial point cloud \mathbf{X} of the mug can be considered non-degenerate if we see points on the cup as well as the handle of the mug. We enforce such a criterion using the predicted semantic keypoints $\hat{\mathbf{y}}$.

For each object, we specify groups of keypoints that characterize different semantic parts of the object. For input \mathbf{X} to be considered non-degenerate, we must have points in \mathbf{X} that are close to all the keypoints, in at least one such group. More formally, for each object, we define a collection of sets $\mathcal{D} = \{\mathbf{G}_l\}_{l=1}^m$, where each set \mathbf{G}_l is a subset of keypoint indices, namely $\mathbf{G}_l \subset [N]$; where, N is the number of semantic keypoints. We say that a set \mathbf{G}_l covers an input point cloud \mathbf{X} if for every keypoint in $\{\hat{\mathbf{y}}[i] \mid i \in \mathbf{G}_l\}$ there is a point \mathbf{x} , in the point cloud \mathbf{X} , that is close to it. We say that an input point cloud \mathbf{X} is non-degenerate if there is at least one set \mathbf{G}_l , in \mathcal{D} , that covers \mathbf{X} . Mathematically, this is given by:

$$\text{nd}(\mathbf{X}, \hat{\mathbf{y}}) = \mathbb{I} \left\{ \bigcup_{l=1}^m \bigcap_{i \in \mathbf{G}_l} \left\{ \min_{\mathbf{x} \in \mathbf{X}} \|\mathbf{x} - \hat{\mathbf{y}}[i]\|_2 < \delta \right\} \right\}, \quad (12)$$

where $\delta > 0$ is a given hyper-parameter. Note that while non-degeneracy was a property of the input in our original definition (3), our implementation (12) uses the predicted model keypoints $\hat{\mathbf{y}}$ to make the determination. In particular, we declare the input-output pair to be non-degenerate if $\text{nd}(\mathbf{X}, \hat{\mathbf{y}}) = 1$.

V. SELF-SUPERVISED TRAINING

This section puts together all the modules introduced in the previous section and introduces our self-supervised training method that allows us to take a simulation-trained model and self-train it to work on real data.

Self-Supervised Loss. We self-supervise the output $\mathbf{y} = \tilde{\mathbf{y}} + \Delta \mathbf{y}^*$ produced by the detector+corrector using the predictions: $\hat{\mathbf{R}}, \hat{\mathbf{t}}, \hat{\mathbf{X}}, \hat{\mathbf{y}}$ (see Fig. 4). We use half-Chamfer loss and keypoint loss for self-supervised training:

$$\mathcal{L} = \text{ch}_{1/2}(\mathbf{X}, \hat{\mathbf{X}}) + \theta \|\mathbf{y} - \hat{\mathbf{y}}\|_2^2, \quad (13)$$

where θ is a positive constant.

Training with Certification. Self-supervised training using the just the loss function (13) does not work. This is because, some of the predicted models $\hat{\mathbf{X}}$ are not correctly registered to the input point clouds \mathbf{X} . Including them in the loss function (13) induces incorrect supervision causing the self-supervised training to fail.

We, therefore, propose to use the certificate of correctness (11) during training. At each iteration, we train on the loss (13) computed only for those input-output pairs that are certifiable (correctness) (11). Certification weeds out incorrectly registered object models during the self-supervised training and provides for correct supervision and weight adjustments to the keypoint detector during training. As training progresses, the certifiable (correctness) input-output pairs increase and the model learns to predict object pose (and model fit) with increasing accuracy on the real data.

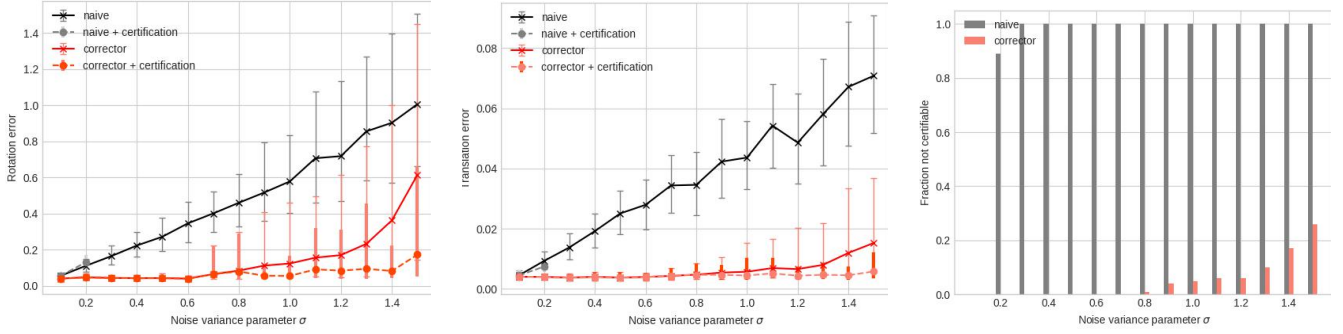
VI. EXPERIMENTS

We present three experiments. We first analyze the ability of the corrector to correct errors in the keypoint detections (Section VI-A). We show the effectiveness of the certification and self-supervised training on a depth-point-cloud dataset generated using ShapeNet [46] objects (Section VI-B). We apply our method on the YCB dataset [1], [2] (Section VI-C).

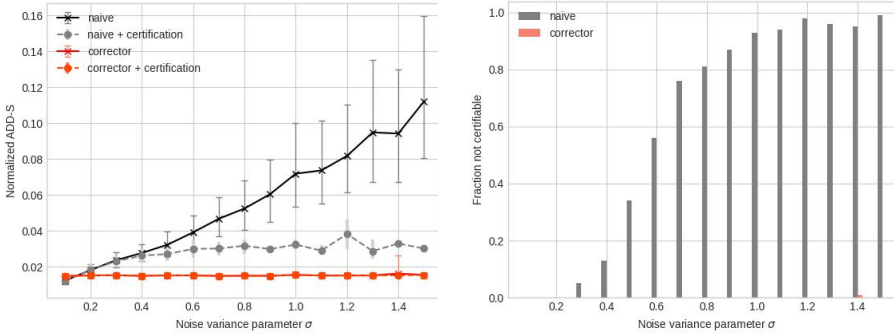
A. Keypoint Corrector Analysis

This section provides a first ablation study and shows that the keypoint corrector module is able to correct large errors in the keypoints detections (*e.g.*, induced by the sim-to-real gap).

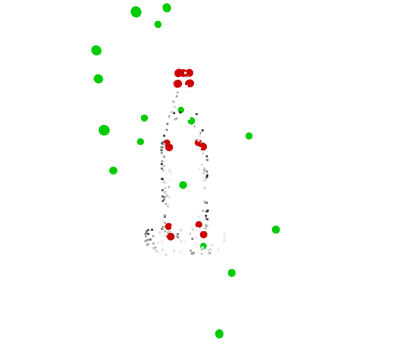
Setup. We consider ShapeNet objects [46] and use the semantic keypoints labeled by the KeypointNet dataset [41]. Give an object model \mathbf{B} with the semantic keypoints \mathbf{b} , we add perturbation to the semantic keypoints, extract depth point cloud of \mathbf{B} from a certain viewing angle, and transform the extracted depth point cloud, along with the perturbed semantic keypoints, by a random pose. We study the performance of the corrector with increasing noise perturbation to the semantic keypoints. We consider the following perturbation model. For



(a) Rotation error (left), translation error (middle), and fraction certifiable (right) as a function of the noise variance parameter σ for an asymmetric chair in ShapeNet.



(b) ADD-S normalized to object diameter (left) and fraction certifiable (right) as a function of the noise variance parameter σ for a symmetric bottle in ShapeNet.



(c) Perturbed keypoints (green) and true keypoints (red) for a symmetric bottle in ShapeNet at $\sigma = 0.8$.

TABLE I: Evaluation for the proposed model and baselines for the ShapeNet experiment.

ADD-S	ADD-S (AUC)	car		chair		helmet		laptop		skateboard		table	
Sim. trained		00.00	00.00	00.00	15.08	00.00	02.70	00.00	02.40	04.00	14.07	00.00	02.84
Sim. trained + ICP		00.00	00.00	00.00	14.06	00.00	02.66	00.00	02.00	02.00	12.90	00.00	03.07
Sim. trained + Corrector		00.00	17.78	68.00	60.86	06.00	21.40	22.00	19.41	52.00	57.20	74.00	54.92
Proposed model		74.00	69.76	100.00	83.75	100.00	74.22	96.00	70.34	98.00	87.31	100.00	73.96
Proposed mode (cert)		100.00	76.28	100.00	83.75	100.00	74.22	96.00	70.34	100.00	87.46	100.00	73.96
Supervised baseline		100.00	85.83	100.00	87.96	100.00	83.50	100.00	87.34	100.00	88.93	100.00	82.17
% certifiable		car		chair		helmet		laptop		skateboard		table	
Sim. trained		00.00		00.00		00.00		00.00		00.00		00.00	
Sim. trained + Corrector		00.00		66.00		14.00		22.00		46.00		76.00	
Proposed model		70.00		100.00		100.00		100.00		98.00		100.00	

each keypoint $\mathbf{b}[i]$, with probability f , we add uniform noise distributed in $[-\sigma d/2, \sigma d/2]$, and with probability $1 - f$, keep $\mathbf{b}[i]$ unperturbed. Here, d is the diameter of the object. We set $f = 0.8$ and see the performance of the corrector as a function of the noise variance parameter σ .

Results. For a chair model in the ShapeNet dataset, Fig. 5a shows the rotation and translation error as a function of the noise variance parameter σ . We compare the output produced by the corrector + registration with a naive method that uses only the registration block (*i.e.*, solves only (1)) using the perturbed keypoints $\tilde{\mathbf{y}}$. Not all outputs produced by these two models — naive and corrector — are certifiably correct per eq. (11). In the figure, we also plot the rotation and translation errors for the fraction of certifiable (correctness) input-outputs. We also show the fraction certifiable (correctness) produced by the naive and

the corrector (rightmost column in the figure). Similar plots for other ShapeNet objects are presented in Appendix C.

Fig. 5a shows that the rotation and translation error is considerably lower, when using the corrector viz-a-vi the naive method. For instance, when we add uniformly distributed noise, distributed in the range $[-d/2, +d/2]$, to 80% of the keypoints, the corrector is still able to correct it and reduce the average rotation error to within 0.1 radians, which is less than 6 degrees. The naive method on the other hand produces an average rotation error of about 0.6 radians or 34 degrees. The translation error, when using the corrector, remains well within $0.01d$ (*i.e.*, 1% of the diameter of the object).

When using the corrector, we observe that more than 90% of the produced outputs remain certifiable, for $\sigma < 1.2$. The naive method, on the other hand, does not produce certifiable

outputs for any $\sigma \geq 0.4$. This shows that the corrector is able to correct most of the induced errors, even for large perturbations. Using the corrector, along with certification, not only reduces the error, but also brings down the variance in the error.

Symmetric Objects. The chair model is asymmetric. We note here that the corrector works also for symmetric objects. We choose a symmetric bottle from the ShapeNet dataset that has 16 keypoints. As rotation error can be ambiguous for symmetric objects, we use ADD-S score [24], normalized to object diameter, to evaluate the corrector + registration output.

Fig. 5b plots the normalized ADD-S score, normalized to the object diameter. We see that the corrector achieves minimal ADD-S score, with almost 100% certifiability, for all choices of σ , while the ADD-S score for the naive method monotonically increases with σ . Note that at $\sigma = 1.5$ we are essentially perturbing 80% of the keypoints by a uniform distribution that uniformly spans 1.5 times the object diameter. See Fig. 5c for a visualization of a typical error induced on the keypoints at $\sigma = 0.8$. We note here that certification does help reduce the ADD-S for the naive registration to some extent. However, this comes at the cost of increasing non certifiable outputs, which reach nearly 100% at $\sigma = 1.2$.

B. The ShapeNet Experiment

This section demonstrates our self-supervised training on depth-point-cloud data generated using ShapeNet [46] objects.

Setup. We evaluate the proposed self-supervised training using object models in ShapeNet [46]. The ShapeNet dataset classifies objects into 16 categories. We select one object in each category. We use uniformly sampled point clouds of these 16 objects as the simulation dataset and a collection of depth point clouds, generated using Open3D [93], as the real-world dataset. We initially train the detector using the simulation dataset, and train it further, on the depth point cloud dataset, in a self-supervised way, as proposed in Section V.

Performance Metrics and Baselines. Table I shows the performance of the proposed model on the depth point cloud dataset, after the self-supervised training, and other baselines for 6 of the 16 objects. We evaluate the performance of the model using threshold ADD-S and ADD-S (AUC) score [24]. ADD-S measures how far the predicted object model \hat{X} is from the ground truth object, whereas threshold ADD-S measures the fraction of outputs, produced by the model, that have ADD-S below the given threshold. The ADD-S (AUC), given a threshold, measures the area under the ADD-S curve up to that threshold. We choose thresholds for the ADD-S and ADD-S (AUC) to be 2% and 5% of the object diameter d .

We report the following baselines in Table I: (i) Simulation-trained keypoint detector (label: Sim. trained), (ii) Simulation-trained keypoint detector + ICP over the entire predicted point cloud \hat{X} and the input point cloud X , (iii) Simulation-trained keypoint detector + corrector, and (iv) Supervised baseline, which is a trained keypoint detector on the depth point cloud dataset with full supervision, that is not available to any other baseline or the proposed model. We use the supervised baseline to mark an upper-bound on the performance of any self-supervised method. In Table I, the keypoint detector is modeled as a point transformer regression model [88].

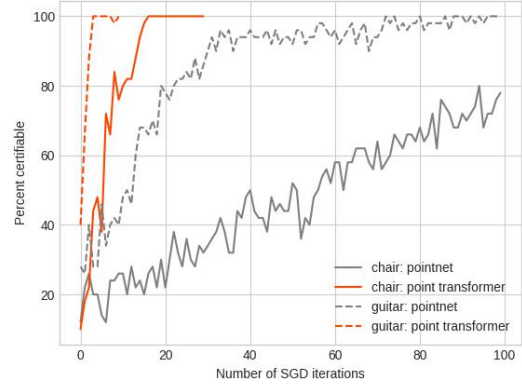


Fig. 6: Percent certifiable (correctness) vs. number of SGD iterations during the proposed self-supervised training.

TABLE II: Proposed model (mug, cap) evaluated for certifiably correct and degenerate cases.

object		ADD-S	ADD-S (AUC)	per-cent
cap	all data	76.00	69.21	100.00
	cert.	77.55	70.59	98.00
	cert.+non-degen.	100.00	84.51	34.00
mug	all data	68.00	62.40	100.00
	cert.	77.27	68.91	88.00
	cert.+non-degen.	100.00	78.91	28.00

Results. Table I shows that the simulation-trained model performs very poorly and is not helped much by ICP. Using the corrector, with the simulation-trained model, yields significant performance improvements. We observe that the ADD-S, ADD-S (AUC), as well as the percent certifiable (correctness) improve considerably, when using the corrector. However, the corrector cannot correct all errors and the performance of the simulation-trained model, with corrector, remains far below the supervised baseline.

The proposed model, with self-supervised training, yields performance very close to the supervised baseline. Also, the percent certifiability moves close to 100%, which means that all the outputs produced by our model, after training, end up being certifiably correct. Appendix D shows that the choice of the neural architecture used for the keypoint detector affects the training time and performance of the proposed model.

Fig. 6 shows how the fraction of certifiable (correctness) outputs increases with the number of SGD iterations during the self-supervised training. The figure plots the results only for two ShapeNet objects (chair and guitar). However, other objects also show a similar trend. We observe that the keypoint detector, when using a point transformer architecture, converges to 100% certifiability much faster than when using a PointNet++ architecture. This is because the PointNet++ detector, when operated on an unseen dataset, induces rotation errors that are not very amenable to correction by the corrector in eq. (6).

Degeneracy. Degeneracy arises when the depth point cloud of an object is occluded enough, so that there are multiple ways to fit the object model to it. We observe this specifically in the case of two objects in the ShapeNet dataset: mug and

TABLE III: Evaluation for the proposed model and baselines for the YCB experiment.

ADD-S	ADD-S (AUC)	master chef can		mustard bottle		banana		scissors		extra large clamp		cracker box	
Sim. trained		00.00	49.46	00.00	57.50	06.67	62.03	27.86	76.70	00.00	51.89	00.00	28.23
Sim. trained + ICP		00.00	49.77	00.00	57.50	00.00	63.20	31.03	77.28	00.00	51.55	00.00	29.66
Sim. trained + Corrector		28.83	62.77	31.83	71.12	70.33	85.01	86.21	89.61	44.81	75.33	28.83	52.41
Proposed model		100.00	91.76	98.83	91.57	99.83	93.43	98.28	93.49	98.08	91.26	59.83	67.99
Proposed mode (cert)		100.00	91.89	99.83	91.90	100.00	93.91	98.16	93.66	98.09	91.31	60.95	68.60
Supervised baseline		68.33	84.39	93.33	87.88	100.00	95.16	93.10	93.37	96.15	91.39	91.67	89.34
% certifiable		master chef can		mustard bottle		banana		scissors		extra large clamp		cracker box	
Sim. trained + Corrector		27.83		27.00		26.00		74.48		27.88		63.67	
Proposed model		92.67		93.33		63.33		94.14		80.96		98.17	

TABLE IV: Proposed model (cracker box) evaluated for certifiably correct and degenerate cases.

cracker box	ADD-S	ADD-S (AUC)	per-cent
all data	59.83	67.99	100.00
cert.	60.95	68.60	98.17
cert.+non-degen.	100.00	92.53	30.00

cap. For the mug, degeneracy occurs when the handle of the mug is not visible, whereas for the cap, when the flap of the cap is not visible (Fig. 2). Table II shows the ADD-S and ADD-S (AUC) scores attained by the proposed model on these two objects (cap and mug). We observe that, while the self-supervised training works correctly to reach 98% certifiability, the ADD-S and ADD-S (AUC) scores remain low. This is because the certifiably correct outputs also include degenerate cases. This causes the predicted output to deviate from the ground truth. In Table II, we also filter the output using the certificate of non-degeneracy in (12) computed in the forward pass. We observe that for the certifiably (correctness) and non-degenerate cases (cert.+non-degen.) we attain high ADD-S, ADD-S (AUC) scores.

C. The YCB Experiment

This section shows the proposed self-training method allows bridging the sim-to-real gap in the YCB dataset [1], [2].

Setup. We use the YCB dataset [1], [2], which is composed of RGB-D images of household objects on a tabletop. The dataset provides Poisson reconstructed meshes, which we use as object models \mathcal{B} . We manually annotate semantic keypoints on each of these objects. For the simulation data, we use uniformly sampled point clouds on \mathcal{B} . The self-training then uses the real RGB-D images from the YCB dataset.

Results. Table III evaluates the proposed model and various other baselines. We list threshold ADD-S and ADD-S (AUC) numbers, along with percent certifiable (correctness). We use 1cm and 5cm as the thresholds for ADD-S and ADD-S (AUC), respectively.

We observe that the simulation-trained detector performs poorly on the real-world dataset and is not helped much by ICP. The ADD-S, ADD-S (AUC), and percent certifiability improves when the simulation-trained detector is used in conjunction with the corrector module. The proposed model, after self-supervised training with certification, is able to match the

supervised baseline that is trained on the real dataset, with full keypoint and pose supervision.

Degeneracy. While the ADD-S and ADD-S (AUC) scores are in the 90s for most objects, this is not the case for the cracker box. The cracker box has a high percentage of certifiably correct outputs, but suffers from low ADD-S and ADD-S (AUC), *i.e.*, the predicted model $\hat{\mathbf{X}}$ does not match the ground truth. This happens because, in many cases, the input point cloud \mathbf{X} has degeneracy (*e.g.*, only 2 sides of the box are visible). We use the non-degeneracy certificate in eq. (12) to separate out the degenerate and non-degenerate cases. Table IV shows that for the certifiably correct and non-degenerate cases the evaluations reach near-perfect scores.

VII. CONCLUSION

We considered the problem of pose estimation and model fitting. We used a semantic-keypoint-based architecture, and amended it with a corrector and a certification module. We implemented the corrector module as a declarative layer, and proved that its back-propagation can be implemented with a very simple gradient. The certification module declares whether the output produced by the model is certifiable (*i.e.*, correct) or not, and also flags uniqueness of the produced solution. We then proposed a new self-supervised training method that uses the corrector, in conjunction with the certification. We observed that the training succeeded in taking a pre-trained model in simulation, to work on real-data without using any annotations. We conducted experiments on the ShapeNet and YCB dataset, and showed the proposed approach achieves performance comparable to a fully supervised baseline while not requiring pose or keypoint supervision on real data.

APPENDIX

A. Proof of Theorem 3

Note that the only places where $\Delta\mathbf{y}$ appears in the corrector is in conjunction with $\tilde{\mathbf{y}}$, and that too, in the form $\tilde{\mathbf{y}} + \Delta\mathbf{y}$ (see (1), (6)). The corrector optimization problem can therefore be written as:

$$\underset{\Delta\mathbf{y}}{\text{minimize}} \quad f(\tilde{\mathbf{y}} + \Delta\mathbf{y}), \quad (14)$$

for some function f , obtained by subsuming the constraints in (6) into the objective function and realizing that $R(\Delta\mathbf{y})$ and $t(\Delta\mathbf{y})$, can in fact be written as $R(\tilde{\mathbf{y}} + \Delta\mathbf{y})$ and $t(\tilde{\mathbf{y}} + \Delta\mathbf{y})$.

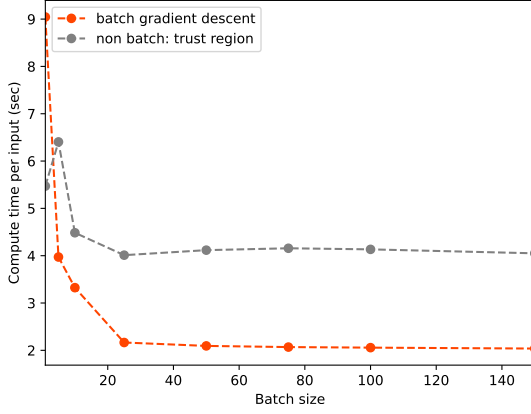


Fig. 7: Compute time (ms) for solving (6) per data point in a batched input, as a function of the batch size.

Let y^* be a solution of the optimization problem $\min_y f(y)$, for f in (14). Then, the optimal correction will be

$$\Delta y^* = y^* - \tilde{y}. \quad (15)$$

Taking derivative with respect to \tilde{y} gives the result.

B. Batch Gradient Descent

The optimization problem in (6) is non-linear and non-convex. A number of open source solvers can be used to solve (6) in the forward pass. We tested different non-linear optimization solvers and observed that two solvers work well, *i.e.*, they are able correct errors in the keypoints by a significant degree. These are a simple constant-step-size gradient descent, which we implement in PyTorch and a trust-region method [94] implemented in SciPy library [95].

A few problems arise in the forward pass implementation of the declarative layer, such as the corrector, during training. Firstly, we train the proposed model with a batch of input data, where each batch may contain 50 – 100 data points, *i.e.*, point clouds. If we use any of the solvers implemented in SciPy or any other open source optimization library, it becomes inevitable to break the batch down and iterate over each data points in the batch, solving the optimization problem (6) for each point in the iteration sequentially. This results in increased training time.

This issue is further exacerbated by the fact that in each such iteration, in which the solver is executed, the data has to be transferred to the CPU in order to solve the optimization problem (6), and then move the solution back to the GPU for further processing. Finally, PyTorch has many optimization algorithms like SGD, ADAM implemented for solving the machine learning problem. These are, however, stochastic in nature and not suited to solve non-linear optimization problems of the type (6). Our tests showed that these solvers do not provide a good solution to the corrector problem.

We, therefore, need a solver for the optimization problem (6) that computes entirely on the GPU, uses the batch processing features in the GPU, and can also solve (6) to a reasonable accuracy. We implement *batch gradient descent* – a simple, fixed step gradient descent implemented in PyTorch that

solves (6) for a batch input, in parallel, without iterating over data points in the batch. This leads to much faster training times and we observe that even with a simple, fixed-step gradient descent, we are able to solve (6) quite accurately.

In Figure 7, we show a comparison of the compute time advantage viz-a-viz a SciPy optimization solver. The figure plots the time taken by a solver to output the solution to (6), per data point in the batch, and a function of the total batch size. We see that with increasing batch size, the implemented batch gradient descent yields an order of magnitude advantage over the SciPy solver.

C. Keypoint Corrector Analysis: Addendum

We study the performance of the corrector across 16 object categories in the ShapeNet dataset [96]. We randomly pick an object in each category and perform the ablation study described in Section VI-A.

Figures 8, 9, 10, and 11 plot ADD-S and percent certifiability as a function of the noise variance parameter σ . In all cases we observe that the corrector is able to correct added noise to the keypoints, even when the noise is comparable to the object diameter. The sub-figures (c) visualizes an instance of keypoint perturbation at $\sigma = 0.8$. And as in Section VI-A, we observe that the corrector reduces variance in ADD-S, while improving the fraction certifiable, very significantly.

D. The ShapeNet and YCB Experiment Addendum

ShapeNet Data Preparation. For each of the randomly selected 16 objects, one in each object category, we generate 5000 point clouds for training, 50 point clouds each for validation and testing, respectively.

YCB Data Preparation. To derive our depth point cloud dataset used in training, we used the given ground truth segmentation masks on the registered depth images, and removed background points not belonging to the object. We removed background points by projecting the given CAD model onto the point cloud and removing points that are farther than 1cm from the CAD model. We also discarded point clouds with less than 500 points. The number of depth point clouds extracted varies across the YCB objects. We generate the train, test, and validation data using a 80 : 20 : 20 split.

To increase the train dataset size and to ensure that the learned model is robust to small changes in the point cloud, we perform data augmentation on the train and validation data. For each depth point cloud, in the train and validation set, we remove a randomly selected 10% of the points, and perturb the rest with Gaussian noise, with a standard deviation of 0.001m. We again remove point clouds that have less than 500 points, from the dataset, after this process.

Hyper-parameters. We describe our choice of learning rate, number of epochs, the ϵ used in certification (Definition 1), and other parameters used during the self-supervised training. We set the maximum number of epochs to be 20 for ShapeNet and 50 for YCB objects. We made two exceptions in the case of ShapeNet, where we observed that the models for car and helmet were still training (*i.e.*, observed continuing decrease in the train and validation loss, and improvement in the percent

TABLE V: Evaluation for the proposed model and baselines for the ShapeNet experiment (Sim. trained* = Sim. trained + ICP, Sim. trained** = Sim. trained + RANSAC + ICP, Sim. trained + corrector* = Sim. trained + corrector + ICP, and Sim. trained + corrector** = Sim. trained + corrector + RANSAC + ICP.)

ADD-S	ADD-S (AUC)	airplane		bathtub		bed		bottle		cap		car	
Sim. trained		00.00	03.50	00.00	02.00	00.00	02.00	00.00	00.00	00.00	00.00	00.00	00.00
Sim. trained*		00.00	02.49	00.00	02.00	00.00	00.00	00.00	00.00	00.00	00.00	00.00	00.00
Sim. trained**		00.00	05.35	00.00	00.00	00.00	00.00	00.00	00.00	00.00	00.00	00.00	00.00
Sim. trained + Corrector		34.00	44.51	16.00	30.82	06.00	28.89	90.00	70.35	26.00	23.17	00.00	17.78
Sim. trained + Corrector*		30.00	44.73	12.00	22.44	10.00	30.95	94.00	73.83	24.00	21.74	00.00	20.36
Sim. trained + Corrector**		26.00	39.00	16.00	28.22	04.00	28.98	96.00	76.09	32.00	28.59	00.00	21.17
Proposed model		100.00	92.20	66.00	63.66	80.00	66.41	100.00	78.93	76.00	69.21	74.00	69.76
Proposed mode (cert)		100.00	92.20	77.50	69.53	79.55	66.38	100.00	77.33	77.50	70.59	100.00	76.28
Supervised baseline		100.00	92.80	100.00	84.32	100.00	83.55	100.00	82.94	100.00	87.11	100.00	85.83
% certifiable		airplane		bathtub		bed		bottle		cap		car	
Sim. trained + Corrector		32.00		26.00		10.00		90.00		40.00		00.00	
Proposed model		100.00		80.00		88.00		100.00		98.00		70.00	

ADD-S	ADD-S (AUC)	chair		guitar		helmet		knife		laptop		motorcycle	
Sim. trained		00.00	15.08	00.00	02.68	00.00	02.70	00.00	02.00	00.00	02.40	00.00	18.68
Sim. trained*		00.00	14.06	00.00	03.45	00.00	02.66	00.00	02.00	00.00	02.00	00.00	19.12
Sim. trained**		00.00	02.00	00.00	03.83	00.00	00.00	02.00	16.00	00.00	00.00	00.00	02.55
Sim. trained + Corrector		68.00	60.86	94.00	75.85	06.00	21.40	58.00	61.91	22.00	19.41	42.00	63.58
Sim. trained + Corrector*		60.00	56.47	96.00	79.10	10.00	25.00	42.00	59.51	24.00	20.73	46.00	48.11
Sim. trained + Corrector**		66.00	61.00	92.00	73.29	14.00	23.52	62.00	68.25	20.00	16.20	40.00	63.54
Proposed model		100.00	83.75	100.00	88.04	100.00	74.22	100.00	89.72	96.00	70.34	100.00	79.28
Proposed mode (cert)		100.00	83.75	100.00	88.04	80.85	74.22	100.00	89.72	96.00	70.34	100.00	79.42
Supervised baseline		100.00	87.96	100.00	92.70	100.00	83.50	100.00	94.45	100.00	87.34	100.00	87.40
% certifiable		airplane		bathtub		bed		bottle		cap		car	
Sim. trained + Corrector		66.00		40.00		14.00		30.00		22.00		38.00	
Proposed model		100.00		100.00		100.00		100.00		100.00		96.00	

ADD-S	ADD-S (AUC)	mug		skateboard		table		vessel	
Sim. trained		00.00	03.05	04.00	14.07	00.00	02.84	00.00	26.40
Sim. trained*		00.00	02.62	02.00	12.90	00.00	03.07	00.00	26.79
Sim. trained**		00.00	00.00	00.00	00.00	02.00	03.24	00.00	00.00
Sim. trained + Corrector		42.00	46.89	52.00	57.20	74.00	54.92	10.00	27.46
Sim. trained + Corrector*		46.00	48.11	60.00	60.52	74.00	55.94	10.00	27.48
Sim. trained + Corrector**		40.00	43.88	64.00	62.34	68.00	51.13	04.00	21.98
Proposed model		68.00	62.40	98.00	87.31	100.00	73.96	100.00	84.76
Proposed mode (cert)		77.27	68.91	100.00	87.46	100.00	73.96	100.00	84.76
Supervised baseline		100.00	82.12	100.00	88.93	100.00	82.17	100.00	89.56
% certifiable		mug		skateboard		table		vessel	
Sim. trained + Corrector		56.00		46.00		76.00		10.00	
Proposed model		88.00		98.00		100.00		100.00	

certifiable). For these two models we set maximum number of epochs to 40. For the learning rate, we used 0.02, momentum to be 0.9, while the training batch size was 50. We did not optimize much over these parameters, but only found ones that worked. We believe some improvement can be expected by exhaustively optimizing these training hyper-parameters.

We observe that correctly setting up the certification parameter ϵ plays a crucial role in correctly training the model in a self-supervised manner. Setting it to too high allows for the model to make and accept errors in training, while setting it to too tight leads to increased training time, as a very small number of input-output pairs remain certifiable, for the simulation trained model with the corrector, at the beginning of the self-supervised training.

We choose ϵ by visually inspecting the simulation trained model, applied on the real-world data, with the corrector. If

all input-output pairs declared by the certifier are correct (*i.e.*, registered object models are correctly aligned with the input point cloud), by visual inspection, and those that were not certifiable are incorrect, we decide that the chosen ϵ is correct. A loose ϵ is spotted if the certifier declares an incorrectly registered object model as certifiable. A too tight ϵ , on the other hand, is spotted if a correctly registered object model is declared not certifiable. Following this procedure, we obtained an ϵ for each object category.

Extended Results. We implement a few other baselines for the extended results: (i) Simulation-trained keypoint detector + registration, followed by an iterative closest point (ICP) on the two point clouds (label: Sim. trained + ICP or Sim. trained*), (ii) Simulation-trained keypoint detector, plus registration with outlier detection using RANSAC, followed by an iterative closest point (ICP) on the two point clouds (label: Sim. trained

TABLE VI: Comparing the keypoint detector architecture (PointNet++ vs Point Transformer) used in the proposed model. (Sim. trained* = Sim. trained + ICP, Sim. trained** = Sim. trained + RANSAC + ICP, Sim. trained + corrector* = Sim. trained + corrector + ICP, and Sim. trained + corrector** = Sim. trained + corrector + RANSAC + ICP.)

Object	ADD-S	ADD-S (AUC)	% cert.	keypoint detector
airplane	58.00	69.57	58.00	PointNet++
	100.00	92.20	100.00	Point Transformer
bathtub	50.00	62.05	86.00	PointNet++
	66.00	63.66	80.00	Point Transformer
bed	70.00	64.69	90.00	PointNet++
	80.00	66.41	88.00	Point Transformer
bottle	100.00	78.55	100.00	PointNet++
	100.00	78.93	100.00	Point Transformer
cap	74.00	67.81	100.00	PointNet++
	76.00	69.21	98.00	Point Transformer
car	60.00	56.89	50.00	PointNet++
	74.00	69.76	70.00	Point Transformer
chair	98.00	82.63	98.00	PointNet++
	100.00	83.75	100.00	Point Transformer
guitar	100.00	87.99	98.00	PointNet++
	100.00	88.04	100.00	Point Transformer
helmet	98.00	73.84	100.00	PointNet++
	100.00	74.22	100.00	Point Transformer
knife	100.00	87.44	76.00	PointNet++
	100.00	89.72	100.00	Point Transformer
laptop	98.00	73.54	98.00	PointNet++
	96.00	70.34	100.00	Point Transformer
motorcycle	96.00	78.77	92.00	PointNet++
	100.00	79.28	96.00	Point Transformer
mug	66.00	60.11	80.00	PointNet++
	68.00	62.40	88.00	Point Transformer
skateboard	98.00	87.42	96.00	PointNet++
	98.00	87.31	98.00	Point Transformer
table	96.00	70.59	98.00	PointNet++
	100.00	73.96	100.00	Point Transformer
vessel	98.00	82.85	98.00	PointNet++
	100.00	84.76	100.00	Point Transformer

+ RANSAC + ICP or Sim. trained**), (iii) Simulation-trained keypoint detector + corrector + registration, followed by an iterative closest point (ICP) on the two point clouds (label: Sim. trained + corrector + ICP or Sim. trained + corrector*), and (iv) Simulation-trained keypoint detector + corrector, plus registration with outlier detection using RANSAC, followed by an iterative closest point (ICP) on the two point clouds (label: Sim. trained + corrector + RANSAC + ICP or Sim. trained + corrector**).

For the ShapeNet dataset, we provide the results for 16 randomly selected objects, one in each object category, in Table V. We observe similar trends as noted in Section VI-B across all the object categories. We observe that additions such as ICP or outlier rejection of perturbed keypoints using RANSAC does not help much. The performance of the proposed model reaches close to that of the supervised baseline in most cases. Among all objects, we observe two cases where

degeneracies occur a bit severely - mug and cap. We report the results for these two cases using the certificate of non-degeneracy in Table II in Section VI-B.

In Section VI-B, we noted that the proposed model works better when we use point transformer for the keypoint detector, as opposed to PointNet++, *i.e.*, the former converges to cent percent certifiability much sooner during training (see Figure 6). In Table VI, we report the ADD-S, ADD-S (AUC), and percentage certifiable for models trained using the point transformer and the PointNet++ architecture. We observe that the point transformer performs better in almost all cases.

For the YCB experiment, we present the extended set of results, for all baselines and all 18 YCB object models, in Table VII. We observe a similar trend as in Table III. We, however, observe quite a few degenerate cases, as opposed to the ShapeNet dataset. These cases arise for different types of boxes, blocks, brick, can and a power drill. For the boxes, degeneracy arises when only one face of the box is visible. Similar degenerate cases are observed for other box-like objects such as brick and blocks. Degeneracy arises in the power drill when only the drill portion is visible, but not its handle. In Table VIII, we report our evaluation for the degenerate cases, with the correctness and non-degeneracy certificates. We observe that while the ADD-S and ADD-S (AUC) numbers are low over all the data, our proposed strong certification (correct and non-degenerate) is able to filter out the degenerate cases, yielding ADD-S scores of 100% and ADD-S (AUC) scores in the 90s.

REFERENCES

- [1] B. Calli, A. Singh, A. Walsman, S. Srinivasa, P. Abbeel, and A. M. Dollar, "The YCB object and Model set: Towards common benchmarks for manipulation research," in *2015 International Conference on Advanced Robotics (ICAR)*, (Istanbul, Turkey), pp. 510–517, IEEE, July 2015.
- [2] B. Calli, A. Walsman, A. Singh, S. Srinivasa, P. Abbeel, and A. M. Dollar, "Benchmarking in Manipulation Research: Using the Yale-CMU-Berkeley Object and Model Set," *IEEE Robotics & Automation Magazine*, vol. 22, pp. 36–52, Sept. 2015.
- [3] T. Hodan, P. Haluza, S. Obdrzalek, J. Matas, M. Lourakis, and X. Zabulis, "T-LESS: An RGB-D Dataset for 6D Pose Estimation of Texture-less Objects," *arXiv:1701.05498 [cs]*, Jan. 2017.
- [4] X. Li, R. Cao, Y. Feng, K. Chen, B. Yang, C.-W. Fu, Y. Li, Q. Dou, Y.-H. Liu, and P.-A. Heng, "A Sim-to-Real Object Recognition and Localization Framework for Industrial Robotic Bin Picking," *IEEE Robotics and Automation Letters*, vol. 7, pp. 3961–3968, Apr. 2022.
- [5] K. Kleeberger, C. Landgraf, and M. F. Huber, "Large-scale 6D Object Pose Estimation Dataset for Industrial Bin-Picking," *arXiv:1912.12125 [cs]*, Dec. 2019.
- [6] B. Drost, M. Ulrich, P. Bergmann, P. Hartinger, and C. Steger, "Introducing MVTEC ITODD — A Dataset for 3D Object Recognition in Industry," in *2017 IEEE International Conference on Computer Vision Workshops (ICCVW)*, (Venice, Italy), pp. 2200–2208, IEEE, Oct. 2017.
- [7] P. Wang, X. Huang, X. Cheng, D. Zhou, Q. Geng, and R. Yang, "The ApolloScape open dataset for autonomous driving and its application," *IEEE Trans. Pattern Anal. Machine Intell.*, 2019.
- [8] P. Sun, H. Kretschmar, X. Dotiwalla, A. Chouard, V. Patnaik, P. Tsui, J. Guo, Y. Zhou, Y. Chai, B. Caine, *et al.*, "Scalability in perception for autonomous driving: Waymo open dataset," in *Proceedings of the IEEE/CVF Conference on Computer Vision and Pattern Recognition*, pp. 2446–2454, 2020.
- [9] H. Caesar, V. Bankiti, A. H. Lang, S. Vora, V. E. Liong, Q. Xu, A. Krishnan, Y. Pan, G. Baldan, and O. Beijbom, "nusenes: A multimodal dataset for autonomous driving," in *Proceedings of the IEEE/CVF conference on computer vision and pattern recognition*, pp. 11621–11631, 2020.

TABLE VII: Evaluation for the proposed model and baselines for the YCB experiment (Sim. trained* = Sim. trained + ICP, Sim. trained** = Sim. trained + RANSAC + ICP, Sim. trained + corrector* = Sim. trained + corrector + ICP, and Sim.trained + corrector** = Sim. trained + corrector + RANSAC + ICP.)

ADD-S	ADD-S (AUC)	chips can		master chef can		cracker box		sugar box		tomato soup can		mustard bottle	
Sim. trained		00.00	33.61	00.00	49.46	00.00	28.23	00.00	37.76	00.00	35.18	00.00	57.50
Sim. trained*		00.00	33.47	00.00	49.77	00.00	29.66	00.00	37.84	00.00	34.84	00.00	57.50
Sim. trained**		00.00	12.38	00.00	21.27	00.00	8.16	00.00	16.72	00.00	11.47	00.00	25.12
Sim. trained + Corrector		63.17	67.00	28.83	62.77	28.83	52.41	37.00	60.09	37.17	78.40	31.83	71.12
Sim. trained + Corrector*		66.67	67.89	25.00	64.26	30.00	51.92	36.67	58.29	40.00	81.85	35.00	72.85
Sim. trained + Corrector**		61.67	65.65	35.00	65.20	30.00	52.81	40.00	62.38	38.33	78.39	23.33	69.53
Proposed model		99.00	90.83	100.00	91.76	59.83	68.16	59.33	76.78	98.17	93.85	98.83	91.57
Proposed mode (cert)		99.08	91.01	100.00	91.89	60.85	68.78	61.63	77.76	100.00	94.27	99.83	91.90
Supervised baseline		100.00	92.01	68.33	84.39	91.67	89.34	53.33	81.70	100.00	92.91	93.33	87.88
% certifiable		chips can		master chef can		cracker box		sugar box		tomato soup can		mustard bottle	
Sim. trained + Corrector		65.50		27.83		63.67		71.83		19.33		27.00	
Proposed model		92.00		92.67		98.33		95.00		75.33		93.33	

ADD-S	ADD-S (AUC)	tuna fish can		pudding box		gelatin box		potted meat can		banana		bleach cleanser	
Sim. trained		05.00	68.20	01.67	46.26	14.21	73.28	00.00	28.05	06.67	62.03	00.00	20.36
Sim. trained*		01.67	68.61	00.00	46.11	14.29	73.22	00.00	27.72	00.00	63.20	00.00	19.60
Sim. trained**		00.00	36.54	00.00	26.39	01.79	32.64	00.00	13.09	01.67	38.18	00.00	07.67
Sim. trained + Corrector		55.33	81.24	52.67	75.66	67.14	85.17	32.83	66.91	70.33	85.01	26.17	63.94
Sim. trained + Corrector*		51.67	80.22	56.67	74.56	69.64	85.58	33.33	67.10	71.67	86.22	23.33	59.94
Sim. trained + Corrector**		70.00	84.75	48.33	73.95	67.86	85.87	31.67	67.49	70.00	85.09	30.00	63.72
Proposed model		100.00	93.86	70.83	86.82	79.82	89.95	74.17	89.47	99.83	93.43	89.67	88.94
Proposed mode (cert)		100.00	94.09	69.75	87.19	78.49	90.24	76.64	90.21	100.00	93.91	91.03	89.45
Supervised baseline		98.33	89.71	85.00	88.46	76.79	86.27	51.67	81.71	100.00	95.16	100.00	92.61
% certifiable		tuna fish can		pudding box		gelatin box		potted meat can		banana		bleach cleanser	
Sim. trained + Corrector		31.67		30.50		51.43		58.50		26.00		27.00	
Proposed model		58.00		71.33		82.32		93.50		63.33		90.83	

ADD-S	ADD-S (AUC)	power drill		wood block		scissors		large clamp		extra large clamp		foam brick	
Sim. trained		23.33	52.09	00.00	37.28	27.86	76.70	00.00	63.80	00.00	51.89	73.33	71.15
Sim. trained*		01.67	52.26	00.00	37.33	31.03	77.28	00.00	63.31	00.00	51.55	10.00	71.27
Sim. trained**		00.00	14.07	00.00	12.42	00.00	36.01	00.00	47.48	01.92	30.44	00.00	03.83
Sim. trained + Corrector		22.67	68.11	50.17	53.57	86.21	89.61	15.38	70.51	44.81	75.33	87.17	87.43
Sim. trained + Corrector*		25.00	70.09	50.00	54.12	86.21	90.15	11.54	68.01	50.00	76.95	88.33	85.97
Sim. trained + Corrector**		23.33	69.34	46.67	51.62	86.21	90.88	11.54	69.48	48.08	75.37	91.67	87.96
Proposed model		82.83	89.90	64.17	59.18	98.28	93.49	97.69	91.83	98.08	91.26	99.50	94.04
Proposed mode (cert)		89.58	91.19	52.63	48.91	98.16	93.66	100.00	92.41	98.09	91.31	99.69	94.98
Supervised baseline		100.00	93.50	100.0	88.01	93.10	93.37	96.15	89.45	96.15	91.39	90.00	85.04
% certifiable		power drill		wood block		scissors		large clamp		extra large clamp		foam brick	
Sim. trained + Corrector		24.33		54.00		74.48		65.38		27.88		18.17	
Proposed model		83.67		62.83		94.14		67.31		80.96		58.33	

- [10] F. Chabot, M. Chaouch, J. Rabarisoa, C. Teuliere, and T. Chateau, "Deep manta: A coarse-to-fine many-task network for joint 2d and 3d vehicle analysis from monocular image," in *Proceedings of the IEEE conference on computer vision and pattern recognition*, pp. 2040–2049, 2017.
- [11] L. Ke, S. Li, Y. Sun, Y.-W. Tai, and C.-K. Tang, "Gsnet: Joint vehicle pose and shape reconstruction with geometrical and scene-aware supervision," in *European Conference on Computer Vision*, pp. 515–532, Springer, 2020.
- [12] A. Kundu, Y. Li, and J. M. Rehg, "3d-rcnn: Instance-level 3d object reconstruction via render-and-compare," in *Proceedings of the IEEE conference on computer vision and pattern recognition*, pp. 3559–3568, 2018.
- [13] J. G. López, A. Agudo, and F. Moreno-Noguer, "Vehicle pose estimation via regression of semantic points of interest," in *2019 11th International Symposium on Image and Signal Processing and Analysis (ISPA)*, pp. 209–214, IEEE, 2019.
- [14] W. Gao and R. Tedrake, "kpm 2.0: Feedback control for category-level robotic manipulation," *IEEE Robotics and Automation Letter (RA-L)*, 2020.
- [15] L. Manuelli, W. Gao, P. Florence, and R. Tedrake, "kpm: Keypoint affordances for category-level robotic manipulation," in *Proc. of the Intl. Symp. of Robotics Research (ISRR)*, 2019.
- [16] G. Pavlakos, X. Zhou, A. Chan, K. G. Derpanis, and K. Daniilidis, "6-dof object pose from semantic keypoints," in *IEEE Intl. Conf. on Robotics and Automation (ICRA)*, 2017.
- [17] A. Dai, A. X. Chang, M. Savva, M. Halber, T. Funkhouser, and M. Nießner, "ScanNet: Richly-annotated 3D Reconstructions of Indoor Scenes," *arXiv:1702.04405 [cs]*, Apr. 2017.
- [18] C. Gümel, A. Dai, and M. Nießner, "ROCA: Robust CAD Model Retrieval and Alignment from a Single Image," *arXiv:2112.01988 [cs]*, Dec. 2021.
- [19] K. Park, T. Patten, and M. Vincze, "Pix2Pose: Pixel-Wise Coordinate Regression of Objects for 6D Pose Estimation," *2019 IEEE/CVF International Conference on Computer Vision (ICCV)*, pp. 7667–7676, Oct. 2019.
- [20] Y. Xiang, T. Schmidt, V. Narayanan, and D. Fox, "PoseCNN: A Convolutional Neural Network for 6D Object Pose Estimation in Cluttered Scenes," *arXiv:1711.00199 [cs]*, May 2018.
- [21] G. Pavlakos, X. Zhou, A. Chan, K. G. Derpanis, and K. Daniilidis, "6-DoF Object Pose from Semantic Keypoints," *arXiv:1703.04670 [cs]*, Mar. 2017.
- [22] Y. Aoki, H. Goforth, R. A. Srivatsan, and S. Lucey, "PointNetLK: Robust & Efficient Point Cloud Registration using PointNet," *arXiv:1903.05711 [cs]*, Apr. 2019.

TABLE VIII: Evaluation of the proposed model with the correctness and non-degeneracy certificates.

Object	ADD-S	ADD-S (AUC)	%	filter
sugar box	59.33	76.78	100.00	all
	61.63	77.76	95.00	cert.
	100.00	94.23	45.33	cert. + non-degen.
	26.50	64.62	49.67	cert. + degen.
pudding box	70.83	86.82	100.00	all
	69.75	87.19	71.33	cert.
	100.00	94.17	39.33	cert. + non-degen.
	32.81	79.21	32.00	cert. + degen.
gelatin box	79.82	89.95	100.00	all
	78.49	90.24	82.32	cert.
	100.00	95.08	46.96	cert. + non-degen.
	49.71	84.98	35.36	cert. + degen.
potted meat can	74.17	89.47	100.00	all
	76.64	90.21	93.50	cert.
	100.00	94.73	45.50	cert. + non-degen.
	54.33	86.51	48.00	cert. + degen.
power drill	82.83	89.90	100.00	all
	89.58	91.19	83.67	cert.
	94.60	93.29	56.83	cert. + non-degen.
	78.81	90.04	26.83	cert. + degen.
wood block	64.17	59.18	100.00	all
	52.63	48.91	62.83	cert.
	100.00	90.58	20.50	cert. + non-degen.
	31.00	30.73	42.33	cert. + degen.
foam brick	99.50	94.04	100.00	all
	99.69	94.98	58.33	cert.
	100.00	95.16	49.33	cert. + non-degen.
	97.50	64.57	09.00	cert. + degen.

[23] A. Avetisyan, A. Dai, and M. Niessner, “End-to-End CAD Model Retrieval and 9DoF Alignment in 3D Scans,” in *2019 IEEE/CVF International Conference on Computer Vision (ICCV)*, (Seoul, Korea (South)), pp. 2551–2560, IEEE, Oct. 2019.

[24] C. Wang, D. Xu, Y. Zhu, R. Martín-Martín, C. Lu, L. Fei-Fei, and S. Savarese, “DenseFusion: 6D Object Pose Estimation by Iterative Dense Fusion,” *arXiv:1901.04780 [cs]*, Jan. 2019.

[25] N. Pereira and L. A. Alexandre, “MaskedFusion: Mask-based 6D Object Pose Estimation,” *arXiv:1911.07771 [cs]*, Mar. 2020.

[26] X. Deng, J. Geng, T. Bretl, Y. Xiang, and D. Fox, “iCaps: Iterative Category-Level Object Pose and Shape Estimation,” *IEEE Robotics and Automation Letters*, vol. 7, pp. 1784–1791, Apr. 2022.

[27] V. N. Nguyen, Y. Hu, Y. Xiao, M. Salzmann, and V. Lepetit, “Templates for 3D Object Pose Estimation Revisited: Generalization to New Objects and Robustness to Occlusions,” Mar. 2022.

[28] K. Park, A. Mousavian, Y. Xiang, and D. Fox, “LatentFusion: End-to-End Differentiable Reconstruction and Rendering for Unseen Object Pose Estimation,” in *Proceedings of the IEEE/CVF Conference on Computer Vision and Pattern Recognition*, pp. 10710–10719, 2020.

[29] J. Tremblay, T. To, B. Sundaralingam, Y. Xiang, D. Fox, and S. Birchfield, “Deep Object Pose Estimation for Semantic Robotic Grasping of Household Objects,” *arXiv:1809.10790 [cs]*, Sept. 2018.

[30] S. Höfer, K. Bekris, A. Handa, J. C. Gamboa, M. Mozifian, F. Golemo, C. Atkeson, D. Fox, K. Goldberg, J. Leonard, C. Karen Liu, J. Peters, S. Song, P. Welinder, and M. White, “Sim2Real in Robotics and Automation: Applications and Challenges,” *IEEE Transactions on Automation Science and Engineering*, vol. 18, pp. 398–400, Apr. 2021.

[31] J. Collins, S. Goel, A. Luthra, L. Xu, K. Deng, X. Zhang, T. F. Y. Vicente, H. Arora, T. Dideriksen, M. Guillaumin, and J. Malik, “ABO: Dataset and Benchmarks for Real-World 3D Object Understanding,” *arXiv:2110.06199 [cs]*, Oct. 2021.

[32] G. Wang, F. Manhardt, J. Shao, X. Ji, N. Navab, and F. Tombari, “Self6D: Self-Supervised Monocular 6D Object Pose Estimation,” *arXiv:2004.06468 [cs]*, Aug. 2020.

[33] G. Wang, F. Manhardt, X. Liu, X. Ji, and F. Tombari, “Occlusion-Aware Self-Supervised Monocular 6D Object Pose Estimation,” *IEEE*

Transactions on Pattern Analysis and Machine Intelligence, pp. 1–1, 2022.

[34] S. Zakharov, W. Kehl, A. Bhargava, and A. Gaidon, “Autolabeling 3D Objects with Differentiable Rendering of SDF Shape Priors,” Tech. Rep. arXiv:1911.11288, arXiv, Apr. 2020.

[35] X. Deng, Y. Xiang, A. Mousavian, C. Eppner, T. Bretl, and D. Fox, “Self-supervised 6D Object Pose Estimation for Robot Manipulation,” in *2020 IEEE International Conference on Robotics and Automation (ICRA)*, pp. 3665–3671, May 2020.

[36] The New York Times, “Self-Driving Uber Car Kills Pedestrian in Arizona, Where Robots Roam,” <https://www.nytimes.com/2018/03/19/technology/uber-driverless-fatality.html>, 2018.

[37] Wired, “Uber’s Self-Driving Car Saw the Woman It Killed, Report Says,” <https://www.wired.com/story/uber-self-driving-crash-arizona-ntsb-report/>, 2018.

[38] The Guardian, “Tesla driver dies in first fatal crash while using autopilot mode,” www.theguardian.com/technology/2016/jun/30/tesla-autopilot-death-self-driving-car-elon-musk, 2016.

[39] The New York Times, “2 killed in driverless tesla car crash, officials say,” 2021.

[40] S. Suwajanakorn, N. Snavely, J. Tompson, and M. Norouzi, “Discovery of latent 3d keypoints via end-to-end geometric reasoning,” *arXiv preprint arXiv:1807.03146*, 2018.

[41] Y. You, Y. Lou, C. Li, Z. Cheng, L. Li, L. Ma, W. Wang, and C. Lu, “KeypointNet: A Large-scale 3D Keypoint Dataset Aggregated from Numerous Human Annotations,” *arXiv:2002.12687 [cs]*, Aug. 2020.

[42] J. Shi, H. Yang, and L. Carlone, “Optimal Pose and Shape Estimation for Category-level 3D Object Perception,” *arXiv:2104.08383 [cs]*, June 2021.

[43] X. Zhou, A. Karpur, L. Luo, and Q. Huang, “StarMap for Category-Agnostic Keypoint and Viewpoint Estimation,” *arXiv:1803.09331 [cs]*, July 2018.

[44] S. Gould, R. Hartley, and D. Campbell, “Deep declarative networks: A new hope,” *arXiv preprint arXiv:1909.04866*, 2019.

[45] A. Agrawal, B. Amos, S. Barratt, S. Boyd, S. Diamond, and J. Z. Kolter, “Differentiable convex optimization layers,” in *Advances in Neural Information Processing Systems (NIPS)*, pp. 9558–9570, 2019.

[46] A. X. Chang, T. Funkhouser, L. Guibas, P. Hanrahan, Q. Huang, Z. Li, S. Savarese, M. Savva, S. Song, H. Su, J. Xiao, L. Yi, and F. Yu, “ShapeNet: An Information-Rich 3D Model Repository,” *arXiv:1512.03012 [cs]*, Dec. 2015.

[47] K. Chen, R. Cao, S. James, Y. Li, Y.-H. Liu, P. Abbeel, and Q. Dou, “Sim-to-Real 6D Object Pose Estimation via Iterative Self-training for Robotic Bin-picking,” *arXiv:2204.07049 [cs]*, Apr. 2022.

[48] H. Yang, W. Dong, L. Carlone, and V. Koltun, “Self-Supervised Geometric Perception,” in *Proceedings of the IEEE/CVF Conference on Computer Vision and Pattern Recognition*, pp. 14350–14361, 2021.

[49] H. Wang, S. Sridhar, J. Huang, J. Valentin, S. Song, and L. J. Guibas, “Normalized object coordinate space for category-level 6d object pose and size estimation,” in *Proceedings of the IEEE/CVF Conference on Computer Vision and Pattern Recognition*, pp. 2642–2651, 2019.

[50] X. Li, Y. Weng, L. Yi, L. Guibas, A. L. Abbott, S. Song, and H. Wang, “Leveraging SE(3) Equivariance for Self-Supervised Category-Level Object Pose Estimation,” *arXiv:2111.00190 [cs]*, Oct. 2021.

[51] Y. He, H. Fan, H. Huang, Q. Chen, and J. Sun, “Towards Self-Supervised Category-Level Object Pose and Size Estimation,” *arXiv:2203.02884 [cs]*, Mar. 2022.

[52] B. D. Lucas and T. Kanade, “An iterative image registration technique with an application in stereo vision,” in *Intl. Joint Conf. on AI (IJCAI)*, pp. 674–679, 1981.

[53] M. Fischler and R. Bolles, “Random sample consensus: a paradigm for model fitting with application to image analysis and automated cartography,” *Commun. ACM*, vol. 24, pp. 381–395, 1981.

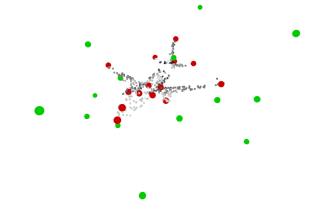
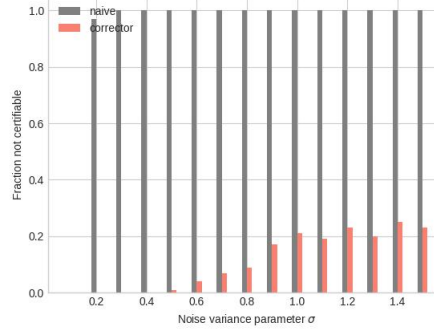
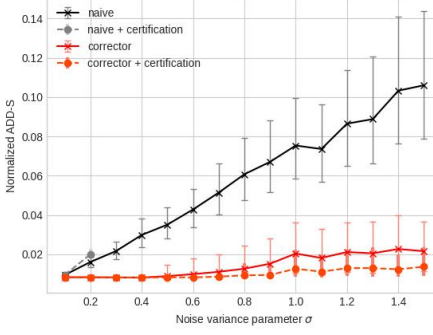
[54] J. Yang, H. Li, D. Campbell, and Y. Jia, “Go-ICP: A globally optimal solution to 3D ICP point-set registration,” *IEEE Trans. Pattern Anal. Machine Intell.*, vol. 38, pp. 2241–2254, Nov. 2016.

[55] A. W. Fitzgibbon, “Robust registration of 2D and 3D point sets,” *Image and Vision Computing*, vol. 21, pp. 1145–1153, Dec. 2003.

[56] S. Bouaziz, A. Tagliasacchi, and M. Pauly, “Sparse iterative closest point,” in *Proceedings of the Eleventh Eurographics/ACMSIGGRAPH Symposium on Geometry Processing*, SGP ’13, (Goslar, DEU), pp. 113–123, Eurographics Association, July 2013.

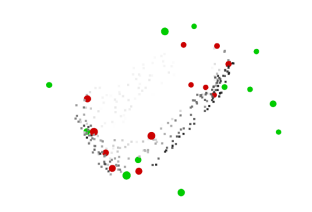
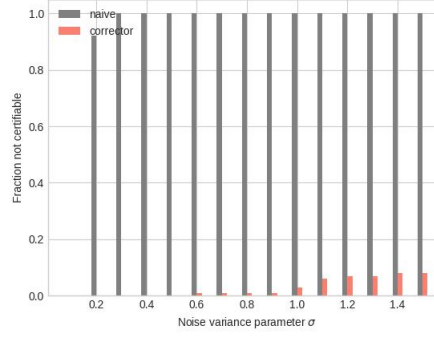
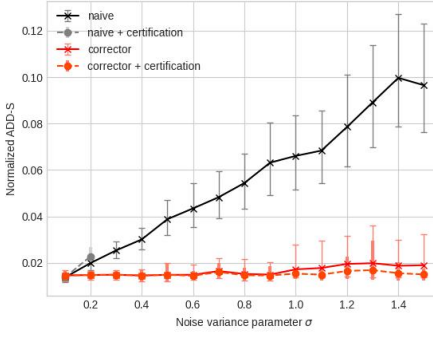
[57] D. Chetverikov, D. Svirko, D. Stepanov, and P. Krsek, “The Trimmed Iterative Closest Point algorithm,” in *2002 International Conference on Pattern Recognition*, vol. 3, pp. 545–548 vol.3, Aug. 2002.

- [58] A. Segal, D. Haehnel, and S. Thrun, "Generalized ICP," https://www.robots.ox.ac.uk/~avsegal/resources/papers/Generalized_ICP.pdf, 2009.
- [59] H. Yang and L. Carlone, "Certifiable Outlier-Robust Geometric Perception: Exact Semidefinite Relaxations and Scalable Global Optimization," *arXiv:2109.03349 [cs, math]*, Sept. 2021.
- [60] J. Shi, H. Yang, and L. Carlone, "ROBIN: A Graph-Theoretic Approach to Reject Outliers in Robust Estimation using Invariants," *arXiv:2011.03659 [cs]*, Mar. 2021.
- [61] P. Antonante, V. Tzoumas, H. Yang, and L. Carlone, "Outlier-Robust Estimation: Hardness, Minimally Tuned Algorithms, and Applications," *arXiv:2007.15109 [cs]*, July 2021.
- [62] H. Yang, J. Shi, and L. Carlone, "TEASER: Fast and Certifiable Point Cloud Registration," *arXiv:2001.07715 [cs, math]*, Oct. 2020.
- [63] H. Yang, P. Antonante, V. Tzoumas, and L. Carlone, "Graduated Non-Convexity for Robust Spatial Perception: From Non-Minimal Solvers to Global Outlier Rejection," *IEEE Robotics and Automation Letters*, vol. 5, pp. 1127–1134, Apr. 2020.
- [64] K. Fu, S. Liu, X. Luo, and M. Wang, "Robust Point Cloud Registration Framework Based on Deep Graph Matching," in *IEEE Conf. on Computer Vision and Pattern Recognition (CVPR)*, pp. 8889–8898, June 2021.
- [65] R. Huang, W. Yao, Y. Xu, Z. Ye, and U. Stilla, "Pairwise Point Cloud Registration using Graph Matching and Rotation-invariant Features," *arXiv:2105.02151 [cs]*, May 2021.
- [66] L. Liu, D. Campbell, H. Li, D. Zhou, X. Song, and R. Yang, "Learning 2D-3D Correspondences To Solve The Blind Perspective-n-Point Problem," *arXiv:2003.06752 [cs]*, Mar. 2020.
- [67] D. Campbell, L. Liu, and S. Gould, "Solving the Blind Perspective-n-Point Problem End-To-End With Robust Differentiable Geometric Optimization," *arXiv:2007.14628 [cs]*, Sept. 2020.
- [68] W. Yuan, B. Eckart, K. Kim, V. Jampani, D. Fox, and J. Kautz, "DeepGMR: Learning Latent Gaussian Mixture Models for Registration," *arXiv:2008.09088 [cs]*, Aug. 2020.
- [69] Z. J. Yew and G. H. Lee, "RPM-Net: Robust Point Matching using Learned Features," *2020 IEEE/CVF Conference on Computer Vision and Pattern Recognition (CVPR)*, pp. 11821–11830, June 2020.
- [70] P.-E. Sarlin, D. DeTone, T. Malisiewicz, and A. Rabinovich, "SuperGlue: Learning feature matching with graph neural networks," in *IEEE Conf. on Computer Vision and Pattern Recognition (CVPR)*, 2020.
- [71] D. DeTone, T. Malisiewicz, and A. Rabinovich, "SuperPoint: Self-Supervised Interest Point Detection and Description," Tech. Rep. *arXiv:1712.07629*, arXiv, Apr. 2018.
- [72] J. Li, C. Zhang, Z. Xu, H. Zhou, and C. Zhang, "Iterative Distance-Aware Similarity Matrix Convolution with Mutual-Supervised Point Elimination for Efficient Point Cloud Registration," *arXiv:1910.10328 [cs]*, Aug. 2020.
- [73] X. Huang, G. Mei, and J. Zhang, "Feature-Metric Registration: A Fast Semi-Supervised Approach for Robust Point Cloud Registration Without Correspondences," in *2020 IEEE/CVF Conference on Computer Vision and Pattern Recognition (CVPR)*, (Seattle, WA, USA), pp. 11363–11371, IEEE, June 2020.
- [74] S. Huang, Z. Gojcic, M. Usvyatsov, A. Wieser, and K. Schindler, "PREDATOR: Registration of 3D Point Clouds with Low Overlap," Nov. 2020.
- [75] Y. Wang and J. M. Solomon, "Deep Closest Point: Learning Representations for Point Cloud Registration," in *Intl. Conf. on Computer Vision (ICCV)*, 2019.
- [76] Y. Li, G. Wang, X. Ji, Y. Xiang, and D. Fox, "DeepIM: Deep Iterative Matching for 6D Pose Estimation," in *Proceedings of the European Conference on Computer Vision (ECCV)*, pp. 683–698, 2018.
- [77] Y. Wang and J. M. Solomon, "PRNet: Self-Supervised Learning for Partial-to-Partial Registration," in *Advances in Neural Information Processing Systems (NIPS)*, pp. 8812–8824, 2019.
- [78] Z. Yew and G. Lee, "3dfeat-net: Weakly supervised local 3d features for point cloud registration," in *European Conf. on Computer Vision (ECCV)*, 2018.
- [79] D. Liu, C. Chen, C. Xu, R. Qiu, and L. Chu, "Self-supervised Point Cloud Registration with Deep Versatile Descriptors," *arXiv:2201.10034 [cs]*, Jan. 2022.
- [80] M. E. Banani, L. Gao, and J. Johnson, "UnsupervisedR&R: Unsupervised Point Cloud Registration via Differentiable Rendering," Feb. 2021.
- [81] H. Yang and L. Carlone, "Certifiably optimal outlier-robust geometric perception: Semidefinite relaxations and scalable global optimization," *IEEE Trans. Pattern Anal. Machine Intell.*, 2021. (pdf).
- [82] A. Bandeira, "A note on probably certifiably correct algorithms," *arXiv:1509.00824*, 2015.
- [83] H. Yang, J. Shi, and L. Carlone, "TEASER: Fast and Certifiable Point Cloud Registration," *IEEE Trans. Robotics*, vol. 37, no. 2, pp. 314–333, 2020. extended arXiv version 2001.07715 (pdf).
- [84] H. Yang and L. Carlone, "In Perfect Shape: Certifiably Optimal 3D Shape Reconstruction From 2D Landmarks," in *2020 IEEE/CVF Conference on Computer Vision and Pattern Recognition (CVPR)*, (Seattle, WA, USA), pp. 618–627, IEEE, June 2020.
- [85] M. Garcia-Salguero, J. Briales, and J. Gonzalez-Jimenez, "Certifiable relative pose estimation," *Image and Vision Computing*, vol. 109, p. 104142, 2021.
- [86] C. R. Qi, L. Yi, H. Su, and L. J. Guibas, "PointNet++: Deep Hierarchical Feature Learning on Point Sets in a Metric Space," *arXiv:1706.02413 [cs]*, June 2017.
- [87] C. R. Qi, H. Su, K. Mo, and L. J. Guibas, "PointNet: Deep Learning on Point Sets for 3D Classification and Segmentation," *arXiv:1612.00593 [cs]*, Apr. 2017.
- [88] H. Zhao, L. Jiang, J. Jia, P. Torr, and V. Koltun, "Point Transformer," *arXiv:2012.09164 [cs]*, Dec. 2020.
- [89] B. Horn, H. Hilden, and S. Negahdaripour, "Closed-form solution of absolute orientation using orthonormal matrices," *J. Opt. Soc. Amer.*, vol. 5, no. 7, pp. 1127–1135, 1988.
- [90] K. Arun, T. Huang, and S. Blostein, "Least-squares fitting of two 3-D point sets," *IEEE Trans. Pattern Anal. Machine Intell.*, vol. 9, pp. 698–700, sept. 1987.
- [91] G. Wahba, "A least squares estimate of satellite attitude," *SIAM review*, vol. 7, no. 3, pp. 409–409, 1965.
- [92] A. Paszke, S. Gross, F. Massa, A. Lerer, J. Bradbury, G. Chanan, T. Killeen, Z. Lin, N. Gimelshein, L. Antiga, A. Desmaison, A. Kopf, E. Yang, Z. DeVito, M. Raison, A. Tejani, S. Chilamkurthy, B. Steiner, L. Fang, J. Bai, and S. Chintala, "Pytorch: An imperative style, high-performance deep learning library," in *Advances in Neural Information Processing Systems 32*, pp. 8024–8035, Curran Associates, Inc., 2019.
- [93] Q.-Y. Zhou, J. Park, and V. Koltun, "Open3D: A modern library for 3D data processing," *arXiv:1801.09847*, 2018.
- [94] A. R. Conn, N. I. M. Gould, and P. L. Toint, *Trust Region Methods*. Society for Industrial and Applied Mathematics, 2000.
- [95] P. Virtanen, R. Gommers, T. E. Oliphant, M. Haberland, T. Reddy, D. Cournapeau, E. Burovski, P. Peterson, W. Weckesser, J. Bright, S. J. van der Walt, M. Brett, J. Wilson, K. J. Millman, N. Mayorov, A. R. J. Nelson, E. Jones, R. Kern, E. Larson, C. J. Carey, I. Polat, Y. Feng, E. W. Moore, J. VanderPlas, D. Laxalde, J. Perktold, R. Cimrman, I. Henriksen, E. A. Quintero, C. R. Harris, A. M. Archibald, A. H. Ribeiro, F. Pedregosa, P. van Mulbregt, and SciPy 1.0 Contributors, "SciPy 1.0: Fundamental Algorithms for Scientific Computing in Python," *Nature Methods*, vol. 17, pp. 261–272, 2020.
- [96] A. X. Chang, T. Funkhouser, L. Guibas, P. Hanrahan, Q. Huang, Z. Li, S. Savarese, M. Savva, S. Song, H. Su, et al., "Shapenet: An information-rich 3d model repository," *arXiv preprint arXiv:1512.03012*, 2015.



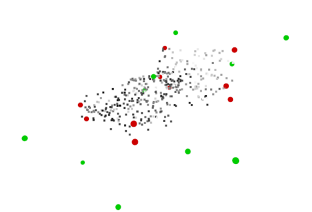
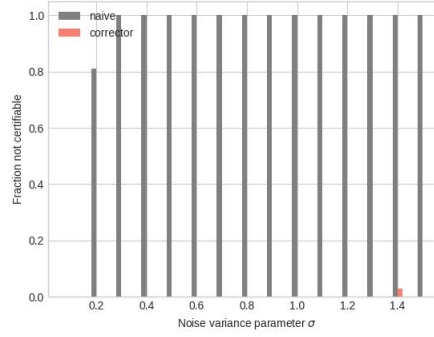
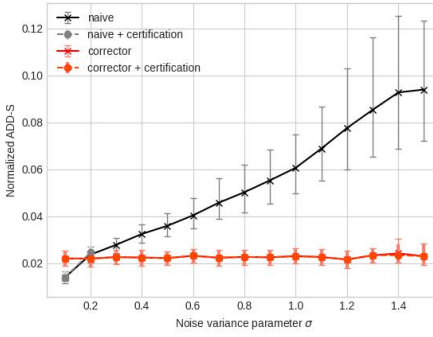
(a) ADD-S normalized to object diameter (left) and fraction certifiable (right) as a function of the noise variance parameter σ .

(b) Perturbed keypoints (green) and true keypoints (red) at $\sigma = 0.8$.



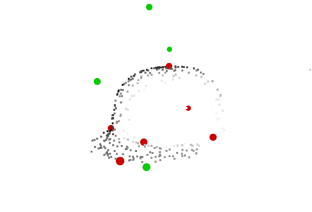
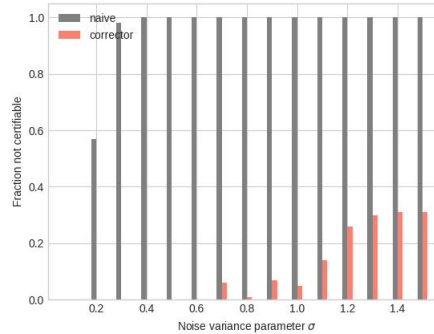
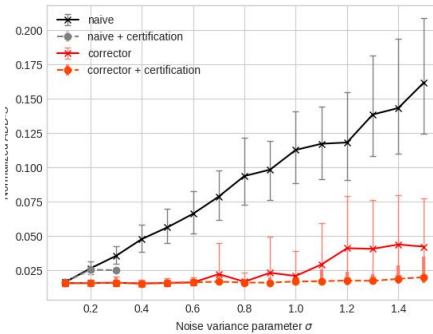
(c) ADD-S normalized to object diameter (left) and fraction certifiable (right) as a function of the noise variance parameter σ .

(d) Perturbed keypoints (green) and true keypoints (red) at $\sigma = 0.8$.



(e) ADD-S normalized to object diameter (left) and fraction certifiable (right) as a function of the noise variance parameter σ .

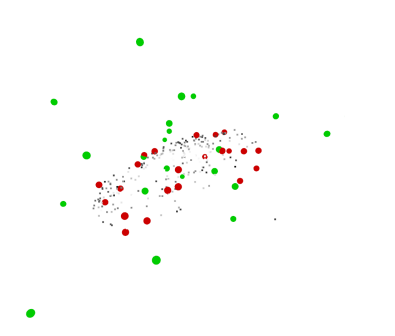
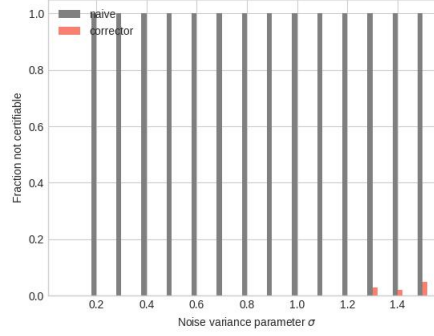
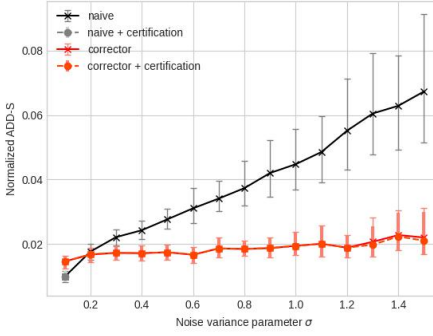
(f) Perturbed keypoints (green) and true keypoints (red) at $\sigma = 0.8$.



(g) ADD-S normalized to object diameter (left) and fraction certifiable (right) as a function of the noise variance parameter σ .

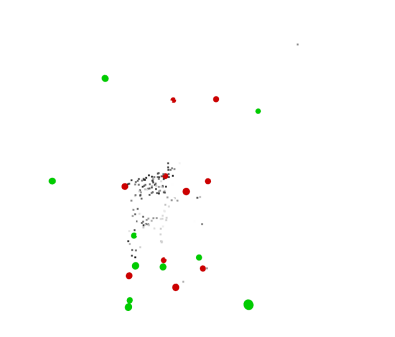
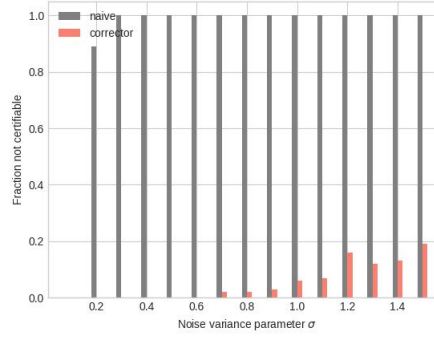
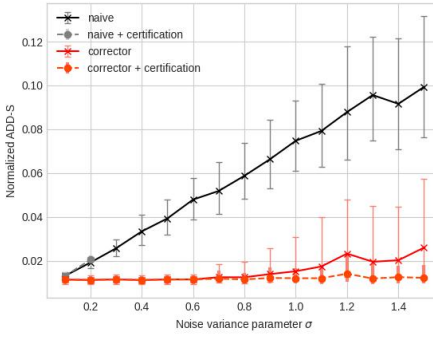
(h) Perturbed keypoints (green) and true keypoints (red) at $\sigma = 0.8$.

Fig. 8: ShapeNet objects: airplane (8a-8b), bathtub (8c-8d), bed (8e-8f), cap (8g-8h).



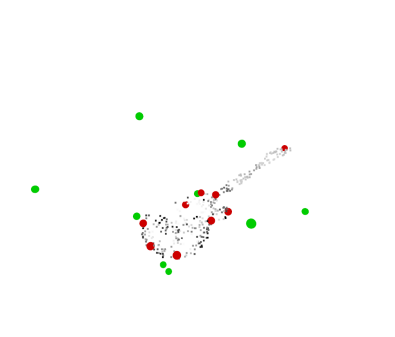
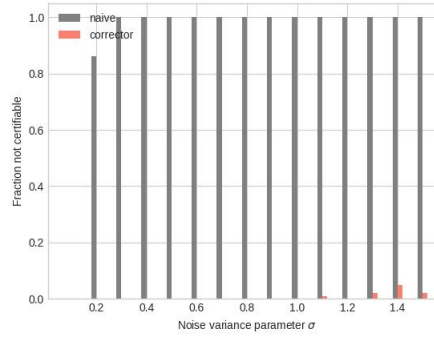
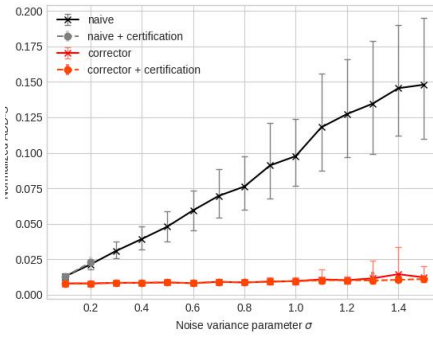
(a) ADD-S normalized to object diameter (left) and fraction certifiable (right) as a function of the noise variance parameter σ .

(b) Perturbed keypoints (green) and true keypoints (red) at $\sigma = 0.8$.



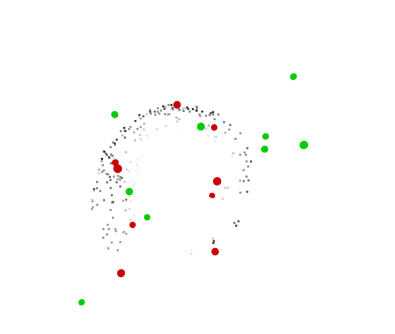
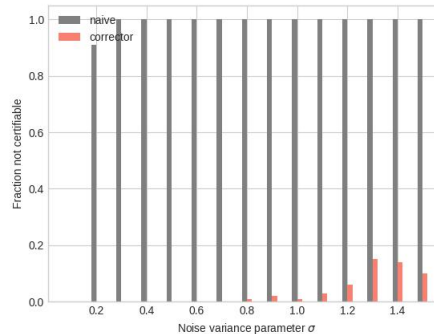
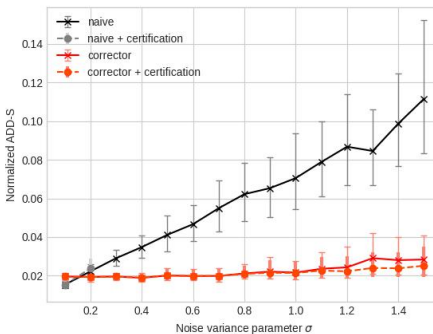
(c) ADD-S normalized to object diameter (left) and fraction certifiable (right) as a function of the noise variance parameter σ .

(d) Perturbed keypoints (green) and true keypoints (red) at $\sigma = 0.8$.



(e) ADD-S normalized to object diameter (left) and fraction certifiable (right) as a function of the noise variance parameter σ .

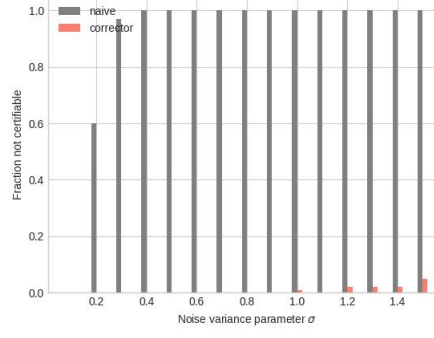
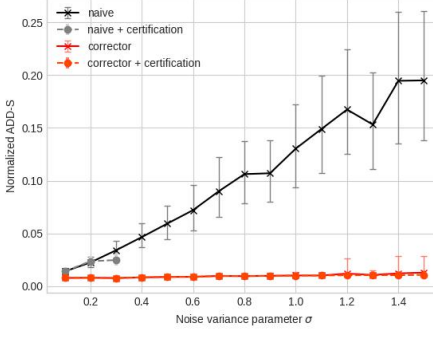
(f) Perturbed keypoints (green) and true keypoints (red) at $\sigma = 0.8$.



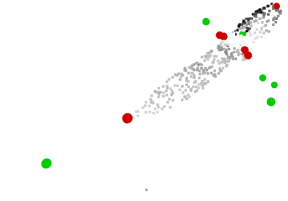
(g) ADD-S normalized to object diameter (left) and fraction certifiable (right) as a function of the noise variance parameter σ .

(h) Perturbed keypoints (green) and true keypoints (red) at $\sigma = 0.8$.

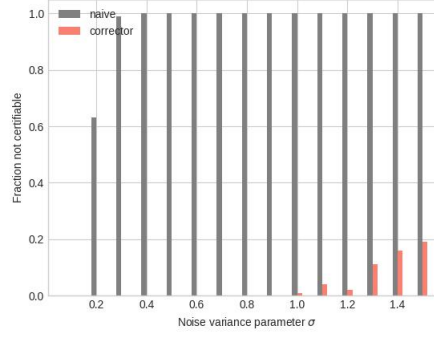
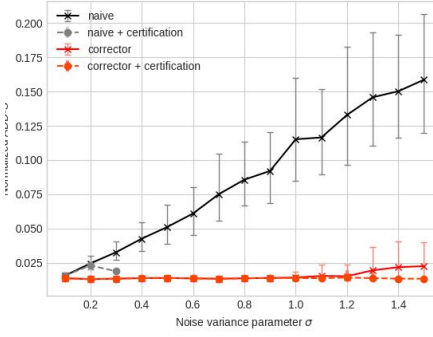
Fig. 9: ShapeNet objects: car (9a-9b), chair (9c-9d), guitar (9e-9f), helmet (9g-9h).



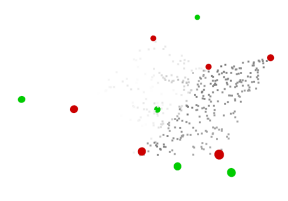
(a) ADD-S normalized to object diameter (left) and fraction certifiable (right) as a function of the noise variance parameter σ .



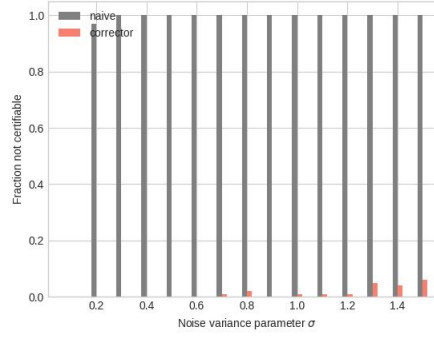
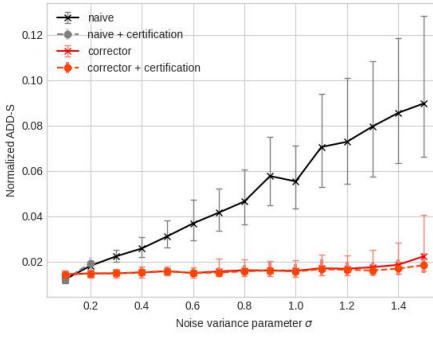
(b) Perturbed keypoints (green) and true keypoints (red) at $\sigma = 0.8$.



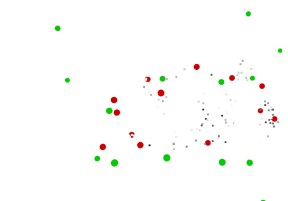
(c) ADD-S normalized to object diameter (left) and fraction certifiable (right) as a function of the noise variance parameter σ .



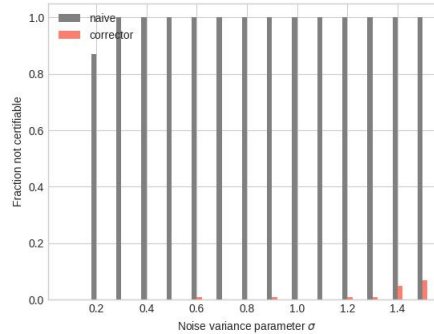
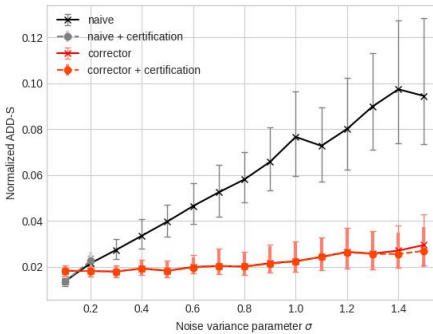
(d) Perturbed keypoints (green) and true keypoints (red) at $\sigma = 0.8$.



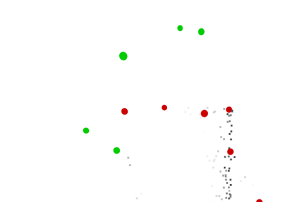
(e) ADD-S normalized to object diameter (left) and fraction certifiable (right) as a function of the noise variance parameter σ .



(f) Perturbed keypoints (green) and true keypoints (red) at $\sigma = 0.8$.

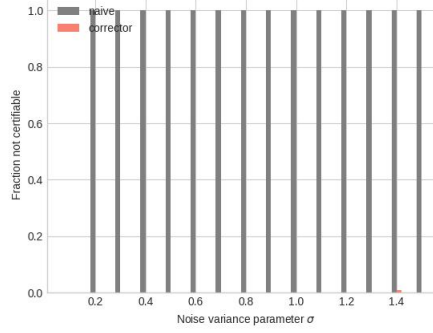
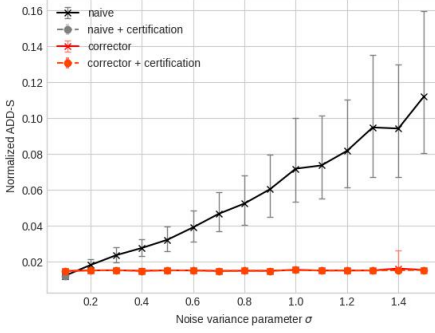


(g) ADD-S normalized to object diameter (left) and fraction certifiable (right) as a function of the noise variance parameter σ .

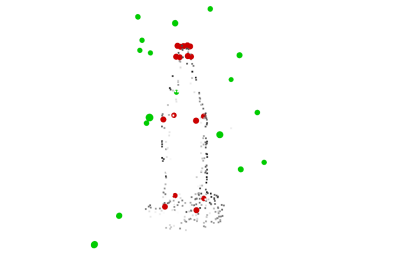


(h) Perturbed keypoints (green) and true keypoints (red) at $\sigma = 0.8$.

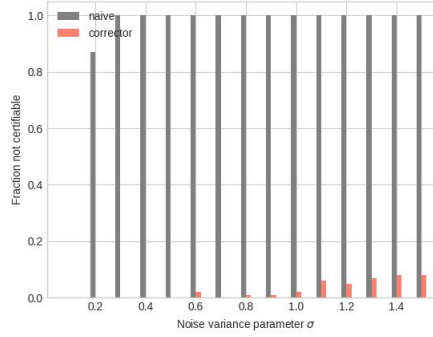
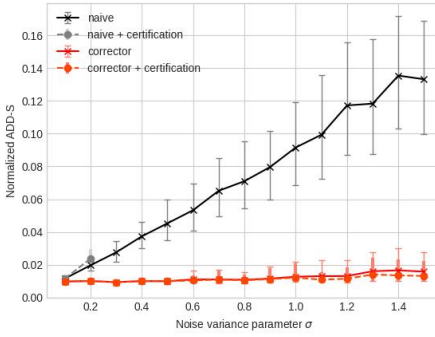
Fig. 10: ShapeNet objects: knife (10a-10b), laptop (10c-10d), motorcycle (10e-10f), mug (10g-10h).



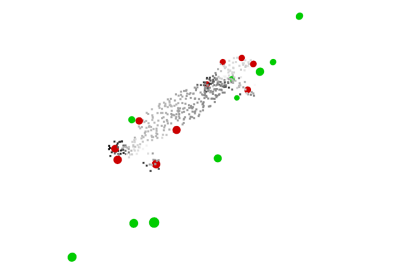
(a) ADD-S normalized to object diameter (left) and fraction certifiable (right) as a function of the noise variance parameter σ .



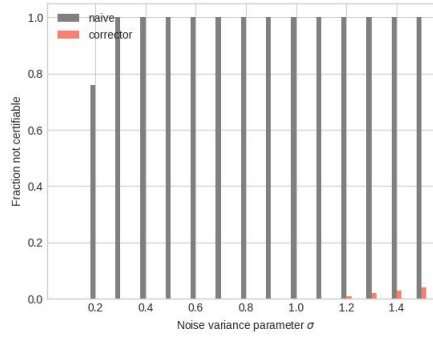
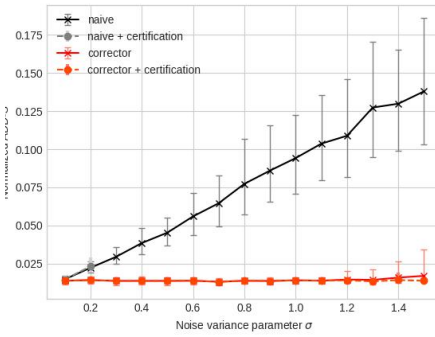
(b) Perturbed keypoints (green) and true keypoints (red) at $\sigma = 0.8$.



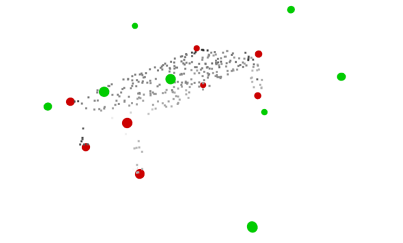
(c) ADD-S normalized to object diameter (left) and fraction certifiable (right) as a function of the noise variance parameter σ .



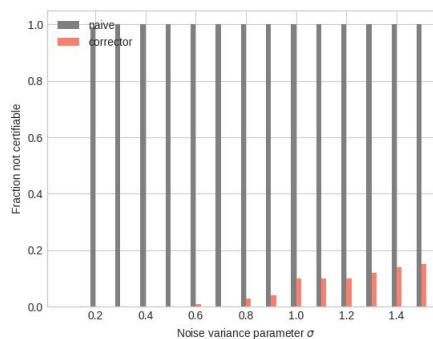
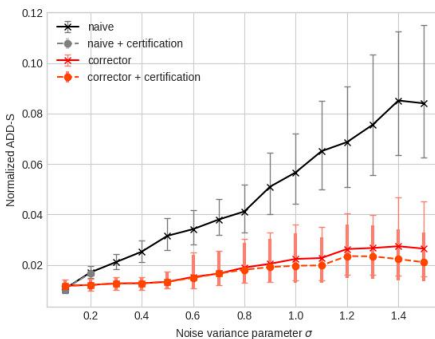
(d) Perturbed keypoints (green) and true keypoints (red) at $\sigma = 0.8$.



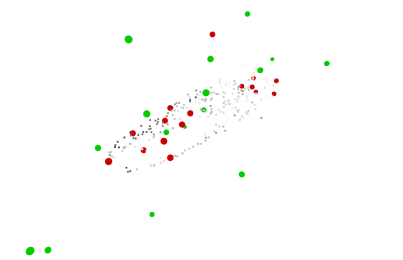
(e) ADD-S normalized to object diameter (left) and fraction certifiable (right) as a function of the noise variance parameter σ .



(f) Perturbed keypoints (green) and true keypoints (red) at $\sigma = 0.8$.



(g) ADD-S normalized to object diameter (left) and fraction certifiable (right) as a function of the noise variance parameter σ .



(h) Perturbed keypoints (green) and true keypoints (red) at $\sigma = 0.8$.

Fig. 11: ShapeNet objects: bottle (11a-11b), skateboard (11c-11d), table (11e-11f), vessel (11g-11h).